Preliminary Results from an Experimental Assessment of a Natural Laminar Flow Design Method

Michelle N. Lynde[1], Richard L. Campbell[2], Melissa B. Rivers[3], Sally A. Viken[4], David T. Chan[5], A. Neal Watkins[6]
NASA Langley Research Center, Hampton, Virginia, 23681

and
Scott L. Goodliff[7]
Jacobs Technology, Inc., Hampton, Virginia, 23681

A 5.2% scale semispan model of the new Common Research Model with Natural Laminar Flow (CRM-NLF) was tested in the National Transonic Facility (NTF) at the NASA Langley Research Center. The model was tested at transonic cruise flight conditions with Reynolds numbers based on mean aerodynamic chord ranging from 10 to 30 million. The goal of the test was to experimentally validate a new design method, referred to as Crossflow Attenuated NLF (CATNLF), which shapes airfoils to have pressure distributions that delay transition on wings with high sweep and Reynolds numbers. Additionally, the test aimed to characterize the NTF laminar flow testing capabilities, as well as establish best practices for laminar flow wind tunnel testing. Preliminary results regarding the first goal of validating the new design method are presented in this paper. Experimental data analyzed in this assessment include surface pressure data and transition images. The surface pressure data acquired during the test agree well with computational fluid dynamics (CFD) results. Transition images at a variety of Reynolds numbers and angles of attack are presented and compared to computational transition predictions. The experimental data are used to assess transition due to a turbulent attachment line, as well as crossflow and Tollmien-Schlichting modal instabilities. Preliminary results suggest the CATNLF design method is successful at delaying transition on wings with high sweep. Initial analysis of the transition front images showed transition Reynolds numbers that exceed historic experimental values at similar sweep angles.

Nomenclature

Acronyms

BLSTA3D	=	Boundary Layer code for Stability Analysis 3D, boundary layer profile solver
CATNLF	=	Crossflow Attenuated Natural Laminar Flow
CDISC	=	Constrained Direct Iterative Surface Curvature, design module
CF	=	Crossflow
CRM	=	Common Research Model
CRM-NLF	=	Common Research Model with Natural Laminar Flow
ESP	=	Electronically Scanned Pressure
FMS	=	Force Measurement System
LASTRAC	=	Langley Stability and Transition Analysis Code, transition prediction software
LFC	=	Laminar flow control
NASA	=	National Aeronautics and Space Administration
NF	=	N-factor

[1] Research Aerospace Engineer, NASA Langley Research Center, Mail Stop 499, Hampton, VA 23681, AIAA Member.
[2] Senior Research Engineer, NASA Langley Research Center, Mail Stop 499, Hampton, VA 23681, AIAA Associate Fellow.
[3] Senior Research Engineer, NASA Langley Research Center, Mail Stop 267, Hampton, VA 23681, AIAA Associate Fellow.
[4] Research Aerospace Engineer, NASA Langley Research Center, Mail Stop 499, Hampton, VA 23681, AIAA Associate Fellow.
[5] Research Aerospace Engineer, NASA Langley Research Center, Mail Stop 499, Hampton, VA 23681, AIAA Senior Member.
[6] Research Scientist, NASA Langley Research Center, Mail Stop 493, Hampton, VA 23681, AIAA Senior Member.
[7] Test Engineer, Jacobs Technology, Inc., Mail Stop 267, Hampton, VA 23681, AIAA Senior Member.

NLF = Natural laminar flow
NTF = National Transonic Facility
SMSS = Sidewall Model Support System
TetrUSS = Tetrahedral Unstructured Software System, flow solver package
TS = Tollmien-Schlichting
TSP = Temperature sensitive paint
TWICS = Transonic Wall Interference Correction System
USM3D = Unstructured Mesh 3D, Navier-Stokes flow solver
VMS = Video Measurement System

Symbols

α = Angle of attack
c = Chord length
C_P = Pressure coefficient
M_{CFD} = Mach number for CFD data
M_{WT} = Mach number for wind tunnel data
mil = Thousandth of an inch, 1 mil = 0.001 inch
μin = Microinch, 1 μin = 0.000001 inch
P_T = Total Pressure
q_∞ = Dynamic pressure
Re_θ = Reynolds number based on attachment line boundary layer momentum thickness
Re_c = Reynolds number based on local chord length
Re_{ft} = Reynolds number based on 1 foot
Re_{MAC} = Reynolds number based on mean aerodynamic chord
Re_t = Reynolds number based on chordwise transition location
T_T = Total temperature
x/c = x-location nondimensionalized by local chord
$(x/c)_t$ = x-location of transition nondimensionalized by local chord
z/c = z-location nondimensionalized by local chord
η = Semispan location nondimensionalized by semispan length
Λ_{LE} = Leading-edge sweep

I. Introduction

ECONOMIC and environmental factors motivate the aerospace industry to continually develop more efficient vehicles. Aircraft designers creating next generation vehicles work to incorporate promising technologies that reduce fuel burn and lower emissions. Maintaining laminar flow on aerodynamic surfaces is one such technology that offers the potential to significantly improve performance through reduced drag. Laminar flow reduces the skin friction and profile drag of a vehicle component, but is sensitive to surface imperfections and can lead to increased wave drag compared to a fully-turbulent vehicle. To make the technology feasible for use on next generation vehicles, aircraft designers must trade the benefits of laminar flow against any negative impacts on cost or performance.

Historically, natural laminar flow (NLF) technology has been limited to aerodynamic surfaces with low sweep and/or low Reynolds number, such as winglets, nacelles [1], or lower speed aircraft wings [2]. This limitation is primarily due to the growth of crossflow instabilities that often lead to boundary layer transition very near the leading edge on surfaces with increased sweep [3]. To support laminar flow on these components, such as the wings of typical commercial transports, a laminar flow control (LFC) system has commonly been needed [4]. One such LFC technology that addresses the growth of crossflow instabilities near the leading edge is boundary layer suction. Suction systems and other LFC technologies have proven to delay boundary layer transition, leading to the known performance benefits associated with significant extents of laminar flow. However, these LFC systems also introduce penalties, such as added weight, system complexity, and cost, that often limit the practicality of applying these technologies to vehicles. An NLF system that controls the rapid growth of crossflow on highly swept wings is one way to maximize the benefits of laminar flow while minimizing the penalties.

The current research is focused on developing, applying, and experimentally validating a new NLF technology that offers the reduced skin friction and profile drag associated with laminar flow without the historic limitations or penalties. The technology, referred to as Crossflow Attenuated Natural Laminar Flow (CATNLF), is a design method that uses geometry shaping to obtain surface pressures that attenuate the crossflow growth very near the leading edge.

The CATNLF design method has been applied to a variety of vehicles in several computational studies at both transonic and supersonic flight conditions [5,6].

A wind tunnel test investigating the successfulness of the CATNLF method to delay boundary layer transition has been conducted to experimentally validate the computational predictions. The new NLF technology has been incorporated into a wind tunnel model, referred to as the Common Research Model with Natural Laminar Flow (CRM-NLF) [7], that has been tested in the National Transonic Facility (NTF) at the NASA Langley Research Center. The wind tunnel test had three primary goals:

1. Validate the CATNLF design methodology and analysis tools
2. Characterize the NTF laminar flow testing capabilities
3. Establish best practices for laminar flow wind tunnel testing

The wind tunnel test of the CRM-NLF model concluded in October of 2018. This paper will present some preliminary findings of this test, focusing primarily on the first goal to experimentally assess the CATNLF technology. A second paper, titled "Experimental Investigation of the NASA Common Research Model with a Natural Laminar Flow Wing in the NASA Langley National Transonic Facility" by Rivers et al., reports additional data from the wind tunnel test [8].

II. CATNLF Technology and Model Design

On wings with sweep and Reynolds number typical of commercial transports, crossflow instabilities grow rapidly very near the leading edge and often lead to boundary layer transition at normal cruise flight conditions. The new CATNLF technology enables laminar flow on swept wings by controlling the growth of these crossflow instabilities through surface pressure architecture. The technology also addresses three other mechanisms of transition: a turbulent attachment line, Görtler vortices, and Tollmien-Schlichting modal instabilities. This section will briefly cover the CATNLF method, computational tools used for design and analysis, and the design of the wind tunnel model.

A. CATNLF Tools and Method

Implementation of laminar flow on vehicles requires additional computational analysis to properly predict the aerodynamic characteristics of the vehicle. For this laminar flow work, the required computational tools include a flow solver, a design module, and boundary layer and stability analysis and transition prediction software. The CATNLF method is built into the design module to be applied and analyzed during the design of an aerodynamic surface (in this application, a transonic wing).

1. Computational Tools

A suite of computational tools is used to apply the CATNLF method to an aerodynamic surface. These tools enable the manipulation of the geometry and the evaluation of transition characteristics. The flow chart in Figure 1 illustrates the design and analysis framework for using the method. The flow chart shows the primary computational tools used for this work in the green blocks.

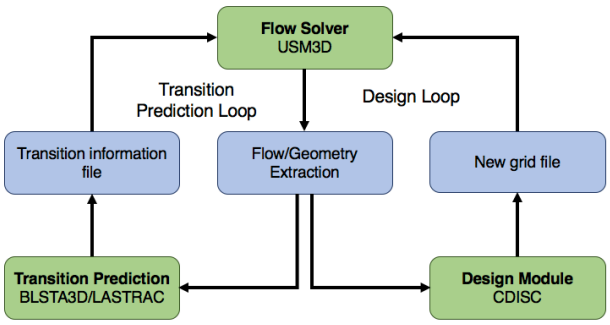

Figure 1. Flow chart showing the NLF design and analysis framework.

The flow solver utilized in this work is USM3D, which is a cell-centered, finite-volume Navier-Stokes code that is part of the TetrUSS package [9]. The grids used with USM3D are unstructured tetrahedral cell grids with a triangular surface mesh. For the computational results provided in this work, a wing-body-horizontal tail configuration is analyzed with a grid of approximately 34.3 million cells, a y+ less than or equal to 0.5 for the first cell off the surface, approximately 30 viscous layers through the boundary layer, and additional refinement in the leading edge region. All the flow solutions in this work use the Spalart-Allmaras turbulence model in regions of turbulent flow and utilize the forced laminarization feature within USM3D to model laminar flow ahead of a designated transition front.

The CATNLF method is built into the CDISC design tool [10]. CDISC is a knowledge-based design tool that is coupled with a flow solver and adjusts the geometry of the aerodynamic surface in order to obtain a target pressure distribution. CDISC flow constraints allow designing to common engineering variables, such as span load, section lift

and pitching moment coefficients, and shock strength. Similarly, geometry constraints are available to address requirements from other disciplines such as structures and manufacturing, including: thickness, curvature, volume, and leading-edge radius. The CDISC design tool has been used for aerodynamic design since the mid-1980s for a variety of configurations and design goals. In this context, the target pressure distribution generated during the CDISC design process incorporates the CATNLF technique for transition delay, detailed in the following subsection. Previous examples of the NLF design capability within CDISC have been reported for both transonic and supersonic configurations [5,6].

The boundary layer and stability analysis and transition prediction software is comprised of two main codes: BLSTA3D [11] and LASTRAC [12]. The BLSTA3D code provides the boundary layer profiles at chordwise stations based on the surface pressure distribution. The conical flow assumption is used when calculating boundary layer profiles to account for wing sweep and taper. BLSTA3D also provides the Reynolds number based on the attachment line boundary layer momentum thickness, Re_θ, which is used to evaluate the attachment line state. LASTRAC is used to perform the stability analysis and transition prediction on the calculated boundary layer profiles. This package allows the user to select from a wide range of fidelity for the stability analysis. For this work, the e^N method is utilized, using linear stability theory with the fixed-beta method and including compressibility effects. Previously published work provides additional detail on the stability analysis method selected for this paper [13]. The computationally predicted transition location is based on a user-supplied critical N-factor, which can be different for crossflow or Tollmien-Schlichting.

2. *Transition Delay Method*

The CATNLF method relies on pressure architecture to control the growth of instabilities that lead to boundary layer transition. For wings with higher sweep like those on typical transport aircraft, the crossflow instabilities grow rapidly very near the leading edge and can cause early transition. If crossflow transition can be avoided, Tollmien-Schlichting instabilities typically become dominant leading to midchord transition. The CATNLF method delays transition by using pressure gradients to reduce the growth of both of these transition mechanisms. An example pressure distribution for a transonic airfoil is shown in Figure 2. Several key features are labeled on the plot that highlight the transition delay technique. The rapid acceleration very near the leading edge keeps the crossflow growth subcritical. Aft of that rapid acceleration, the pressure gradient is tailored to control Tollmien-Schlichting growth such that it gradually increases until it reaches a specified level (the user-supplied critical N-factor) at a desired transition location. A mild adverse pressure gradient is applied from the desired transition location to the shock location to reduce shock strength. Pressures aft of the shock, as well as the lower surface pressures, are determined based on other CDISC constraints, such as pitching moment criteria or thickness requirements.

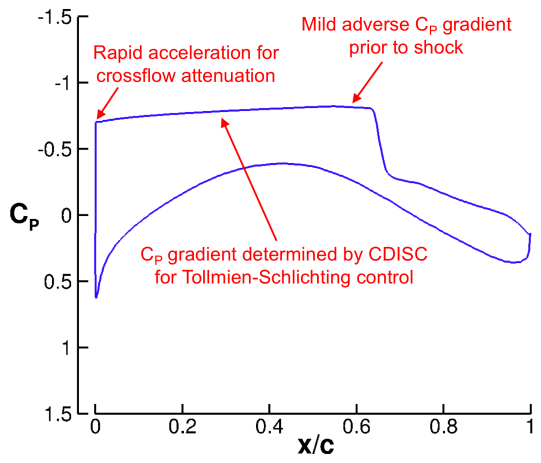

Figure 2. Sample pressure distribution showing key features of the CATNLF design method.

In addition to transition due to crossflow and Tollmien-Schlichting instabilities, the CATNLF method addresses transition due to Görtler vortices and a turbulent attachment line. To avoid Görtler vortices causing transition, a CDISC curvature constraint is applied to avoid concavity in regions of laminar flow. Addressing loss of laminar flow due to a turbulent attachment line has two components that must be avoided: attachment line contamination and attachment line transition. Attachment line contamination is due to a turbulent boundary layer on the fuselage running onto a swept wing and causing the wing attachment line to be turbulent. Attachment line transition is caused when wing characteristics, such as sweep and leading-edge radius, are subject to boundary layer transition. Both attachment line contamination and attachment line transition are evaluated using Poll's criteria [14] based on the Re_θ calculated by the BLSTA3D code. Specific details on the methods used to avoid a turbulent attachment line for the wind tunnel model are described in the following subsection.

B. Model Design

The design of the NLF wind tunnel model that is the subject of this report has been previously documented [7], so only a brief overview will be included here. The baseline configuration for the wind tunnel model is the Common Research Model (CRM) [15,16], which is a generic transonic transport that has been the subject of many studies. The

wind tunnel model is referred to as the Common Research Model with Natural Laminar Flow (CRM-NLF). The design conditions for the model are Mach 0.85, Reynolds number based on mean aerodynamic chord of 30 million, and lift coefficient of 0.50. Figure 3 shows a planform view of the CRM with the chordwise design stations used during the CDISC design process. Two stations, inboard station 6 and outboard station 12 (highlighted in Figure 3), are used to illustrate the geometry and pressure changes needed to obtain NLF. The plots in Figure 4 show these geometry and pressure changes by comparing the baseline CRM (blue, solid line) to the new CRM-NLF (red, dashed line). The key aspects of the CATNLF method can be seen in the CRM-NLF pressure distributions, namely the rapid acceleration for crossflow attenuation and the slightly-favorable pressure gradient needed for Tollmien-Schlichting control. The geometry plots show the necessary changes to the airfoil shapes needed to obtain this NLF pressure distribution. The local twist changes have been removed from the images to highlight the airfoil shape changes. The most notable shape change is in the leading-edge region, where the CRM-NLF has a smaller leading-edge radius. This reduced leading-edge radius helps obtain the rapid acceleration in that region, as well as helps reduce the attachment line Re_θ values. As discussed in the previous subsection, LASTRAC is used to computationally predict the extent of laminar flow based on estimated critical N-factors. A critical N-factor of 10 was selected for the design of the wind tunnel model, which represents a flight environment critical N-factor. The crossflow (CF) and Tollmien-Schlichting (TS) N-factor growth for stations 6 and 12 are shown in Figure 5, demonstrating how the CATNLF pressure distribution technique delays transition.

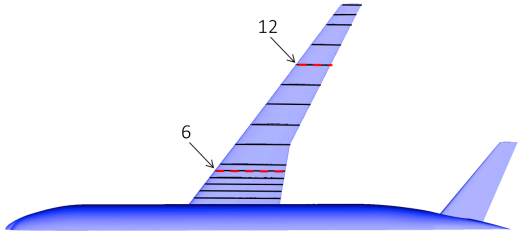

Figure 3. Planform view of the CRM with design stations shown. Stations 6 and 12 are used as example stations in following figures.

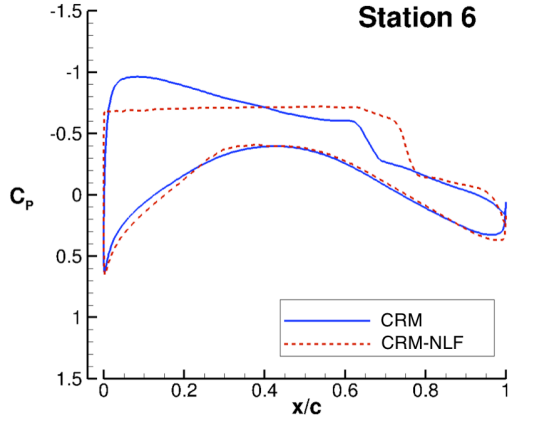

a) Pressure distributions for inboard Station 6.

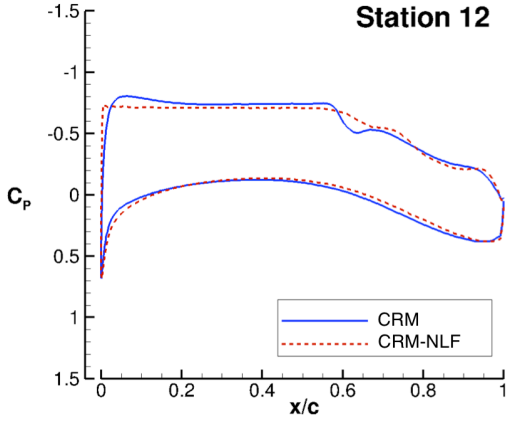

b) Pressure distributions for outboard Station 12.

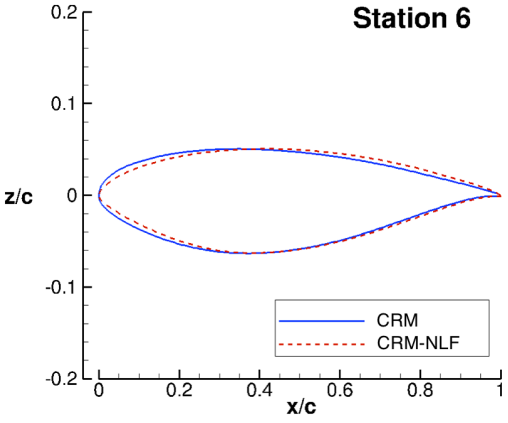

c) Airfoil geometries for inboard Station 6.

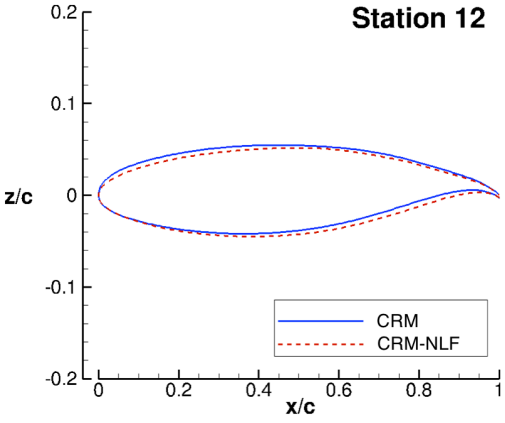

d) Airfoil geometries for outboard Station 12.

Figure 4. Comparison of the pressure distributions and airfoil geometries for the baseline CRM and the new CRM-NLF wing at the design condition of M = 0.86, C_L = 0.50, and Re_{MAC} = 30 million.

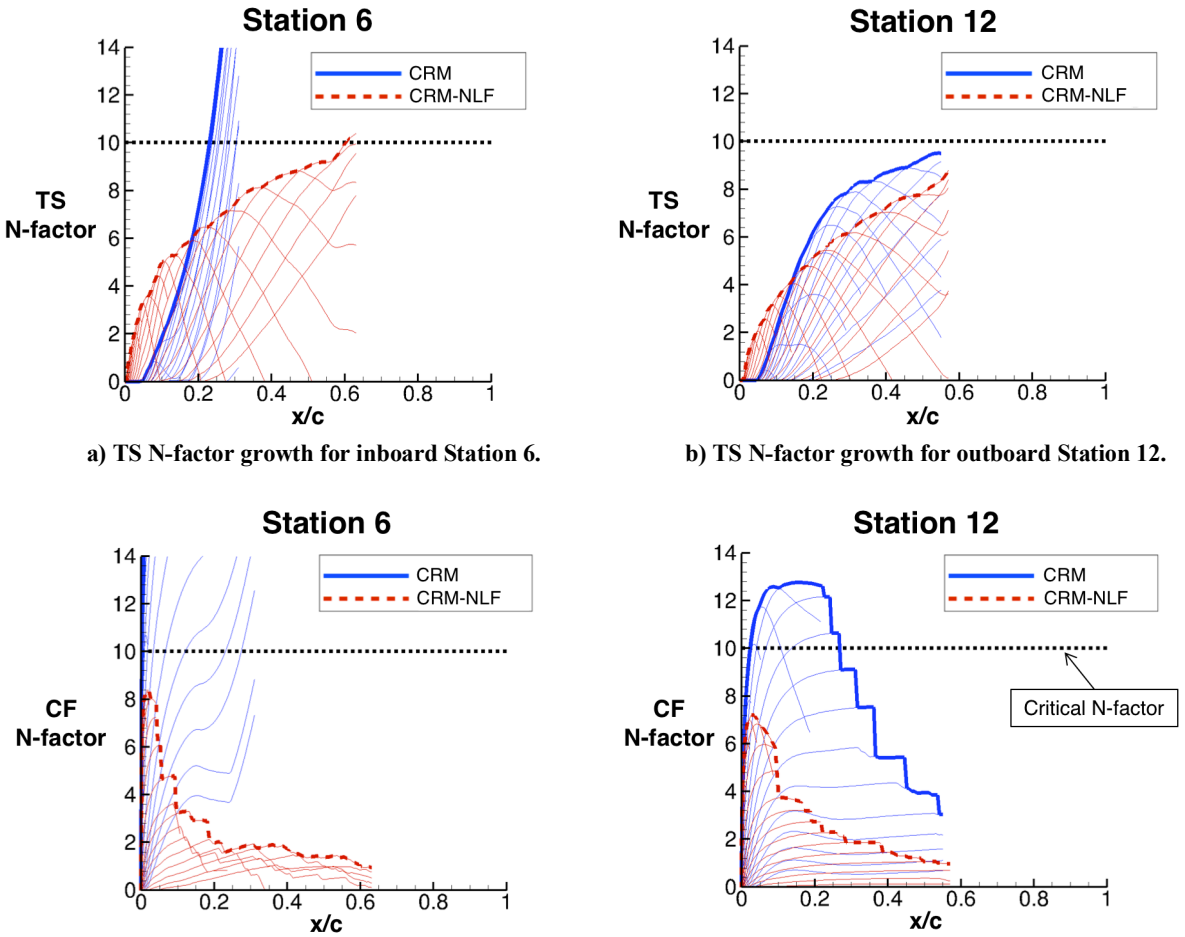

a) TS N-factor growth for inboard Station 6.

b) TS N-factor growth for outboard Station 12.

c) CF N-factor growth for inboard Station 6.

d) CF N-factor growth for outboard Station 12.

Figure 5. Comparison of the crossflow (CF) and Tollmien-Schlichting (TS) N-factor growth for the baseline CRM and the new CRM-NLF wing at the design condition of M = 0.86, C_L = 0.50, and Re_{MAC} = 30 million. The horizontal black dashed line shows the critical N-factor used for the design of the model.

In addition to modal instabilities, the model addresses transition due to Görtler vortices and a turbulent attachment line. Görtler vortices are avoided on this model by imposing a curvature constraint during the design process, which prevents any concavity in the region of the desired laminar flow. To avoid a turbulent attachment line, both attachment line contamination and attachment line transition are considered. The strategy for this model to address attachment line contamination is to relaminarize the attachment line that has become turbulent due to fuselage boundary layer contamination. To relaminarize the attachment line, the inboard Re_θ values are sufficiently low such that relaminarization occurs according to Poll's criteria ($Re_\theta < 100$). The method of reducing the inboard Re_θ values was to reduce the sweep of the inboard 10% span. The planform changes needed for this technique to address attachment line contamination can be seen in Figure 6. Outboard of the reduced sweep section, the attachment line avoids transition by staying below Poll's criteria ($Re_\theta < 235$). Figure 7 shows the spanwise distribution of the calculated Re_θ values at the design condition.

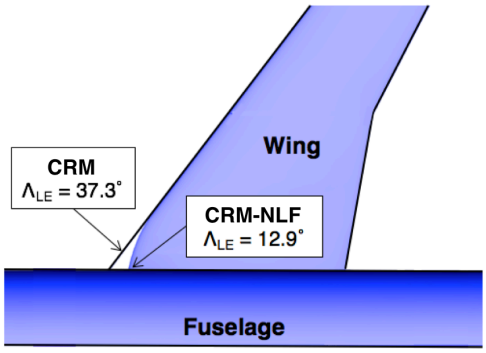

Figure 6. Planform view of the wing-fuselage juncture showing the leading-edge sweep change needed for attachment line control.

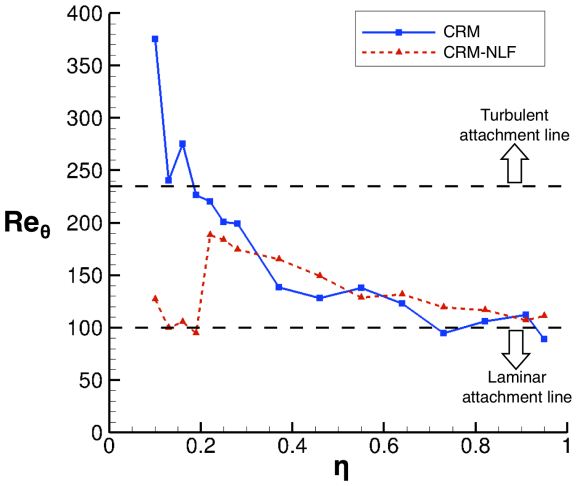

Figure 7. Spanwise distribution of the attachment line Re_θ values for the baseline CRM and the new CRM-NLF at the design condition of M = 0.86, C_L = 0.50, and Re_{MAC} = 30 million.

The predicted transition front for the CRM-NLF wing at the design condition in a flight environment (critical N-factor of 10) is shown in Figure 8 with an estimated 56% of surface area with laminar flow on the wing upper surface. The extent of laminar flow is dependent on the environment, which makes laminar flow testing uniquely challenging. Modern wind tunnels often have significantly higher turbulence levels than flight conditions, which can be represented for computational predictions by reducing the critical N-factor. An example of the environmental dependence of the CRM-NLF on the extent of laminar flow can be seen in Figure 9 where lower critical N-factors correspond to higher turbulence levels. The wind tunnel environment is expected to have a lower critical N-factor than the flight environment design condition, so reducing the test Reynolds number is necessary to increase the extents of laminar flow during the test. Figure 10 demonstrates the increase in predicted laminar flow obtained by reducing the Reynolds number in a constant environment. Previous laminar flow testing at the National Transonic Facility estimated the critical N-factor to be between 4 and 8 for Tollmien-Schlichting transition [17]. For pretest predictions, a critical N-factor of 6 was used for both crossflow and Tollmien-Schlichting transition based on these previous findings. The loading corresponding to the predicted laminar flow extent associated with a critical N-factor of 6 and a Reynolds number based on mean aerodynamic chord of 20 million was used for manufacturing the wing jig-shape.

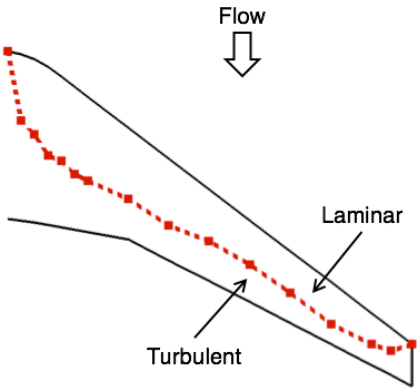

Figure 8. Transition front at the design condition of M=0.85, C_L=0.50, Re_{MAC}=30 million, and critical N-factor of 10.

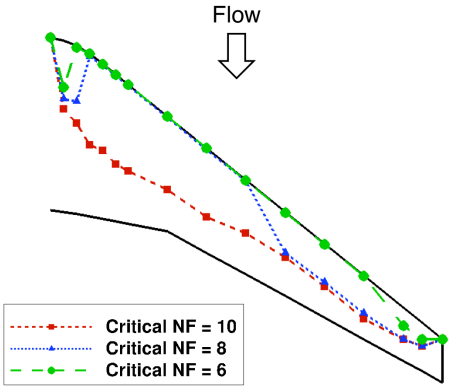

Figure 9. Transition fronts for Re_{MAC}=30 million at different critical N-factors (NF).

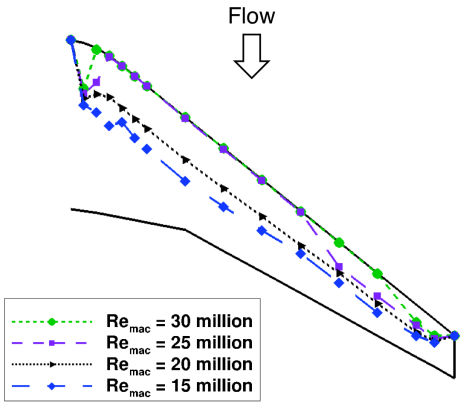

Figure 10. Transition fronts for critical N-factor of 6 at different Re_{MAC} values.

III. Experimental Setup

In order to validate the computational predictions and assess the effectiveness of the CATNLF method in delaying boundary layer transition, an experimental investigation was performed at the National Transonic Facility at the NASA Langley Research Center. This section will briefly cover the experimental setup of the wind tunnel test, including facility details, instrumentation and measurements, and transition visualization techniques. The companion paper titled "Experimental Investigation of the NASA Common Research Model with a Natural Laminar Flow Wing in the NASA Langley National Transonic Facility" by Rivers et al. [8] offers additional detail on the experiment and data collected.

A. Facility Description

Test requirements and goals are considered while selecting a facility to ensure the proposed wind tunnel has the necessary capabilities to achieve those goals. For this laminar flow test, data were needed at transonic speeds, high Reynolds numbers, and acceptably low turbulence levels. The National Transonic Facility (NTF) was selected for this experiment based on the facility's test envelope and previously successful laminar flow tests.

The NTF is a pressurized air and cryogenic wind tunnel capable of reaching flight Reynolds numbers with a semispan model testing capability [18,19]. The facility, illustrated in Figure 11, is a closed-circuit, continuous-flow, fan-driven wind tunnel that enables testing from subsonic to transonic speeds. The wind tunnel controls pressure and temperature separately in order to operate at a wide range of Reynolds numbers. The test section has a slotted floor and ceiling, solid sidewalls, and measures 8.2 by 8.2 by 25 feet. Acoustic treatment both upstream and downstream of the fan minimizes fan-noise effects and thermal insulation inside the pressure shell minimizes heat transfer. The settling chamber has four antiturbulence screens and the contraction ratio from the settling chamber to the nozzle throat is 14.95-to-1. Previous flow measurements have been acquired in the facility to assess the test section unsteady flow environment [20]. These flow measurements, along with a previous natural laminar flow test by Crouch et al. [17], estimated the turbulence intensity in the test section to be approximately 0.24%. The assessment from both of these prior investigations was that the NTF disturbance levels at cryogenic conditions are acceptable for laminar flow testing in the absence of bypass transition. A new test quantifying the test section unsteady flow environment is being conducted to determine if there have been any changes to this turbulence intensity at the tunnel conditions corresponding to the data acquired during this NLF test. The facility can test either fullspan models installed on a sting in the center of the test section, or semispan models installed on the tunnel sidewall. The semispan testing capability was added in the 1990s, and significant effort has recently been completed to improve the data quality and repeatability of semispan tests [21,22,23]. Due to their larger size, semispan models can achieve the same chord Reynolds number as a fullspan model at a lower unit Reynolds number. The boundary layer is thicker at lower unit Reynolds numbers, which is advantageous for laminar flow testing because it reduces the relative height of a particle to the boundary layer. This will aid in decreasing the model's sensitivity to bypass transition due to any particulates in the tunnel.

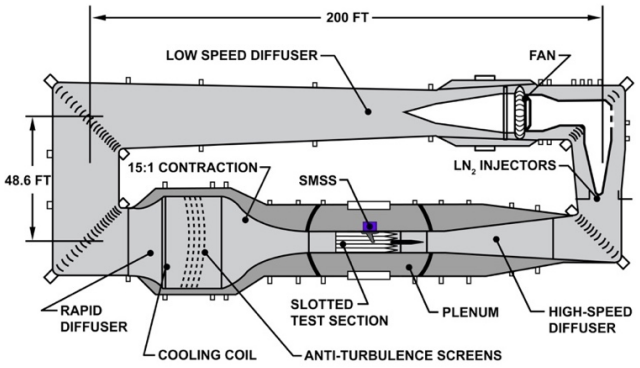

Figure 11. Schematic of the NTF wind tunnel at NASA Langley Research Center.

B. Instrumentation and Measurements

The model, referred to as the Common Research Model with Natural Laminar Flow (CRM-NLF), is a 5.2% scale semispan model, shown installed in the NTF test section in Figure 12. The semispan fuselage hardware was previously tested in the NTF, however, a new wing-fuselage fairing was fabricated to mate with the new CRM-NLF wing. Table 1 lists several model-scale reference parameters.

Table 1. Reference parameters for the CRM-NLF model.

Model-Scale Reference Parameters	
Reference Area	5.584 sq. ft.
Reference Chord	14.342 in.
Semispan Length	60.151 in.
Leading-Edge Sweep (Outboard of Break)	37.3 deg.

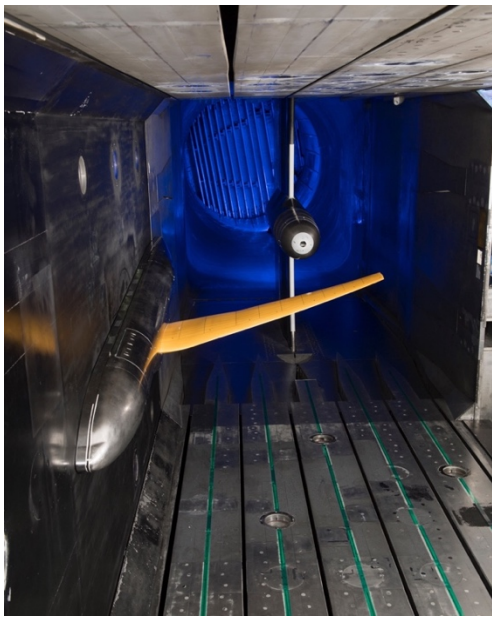

Figure 12. The 5.2% scale semispan model of the CRM-NLF installed in the NTF.

The new CRM-NLF wing was fabricated out of VascoMax C250 steel to withstand the predicted transonic loads in cryogenic conditions. The wing jig shape was derived from finite-element structural analysis such that the wing would deflect into the design shape under the predicted loads. The loads used for the jig-shape design were based on the computational predictions at Mach 0.85, lift coefficient of 0.50, 20 million Reynolds number based on mean aerodynamic chord, dynamic pressure of approximately 1800 psfa, and laminar flow extent associated with a critical N-factor of 6. The model wing was predicted to deflect 1.61 inches at the wingtip during testing under these loads.

The wing was equipped with nine streamwise rows of static pressure ports labeled A through I, as seen in Figure 13. There are a total of 230 pressure ports on the wing: 140 on the upper surface and 90 on the lower surface. In addition to the pressure ports on the wing, the fuselage had 30 static pressure ports connected during the test to assess flow characteristics around the fuselage and monitor any internal flow. The wing pressure ports are arranged in two different layouts, designated Layout A and Layout B, which differ only in the leading-edge region of the upper surface. Figure 14 shows an example of both layouts, and it can be seen that Layout A has pressure ports on the upper surface beginning at x/c = 0.001, while the most forward upper surface pressure tap on Layout B is at x/c = 0.25. Small surface imperfections can cause loss of laminar flow, so pressure ports are typically avoided on surfaces where laminar flow is desired. This is especially true near the leading edge where the boundary layer is much thinner. For the goal of evaluating the CATNLF method, acquiring surface pressure data very near the leading edge was essential to ensure the desired pressure architecture was obtained (primarily the rapid acceleration for crossflow attenuation as seen in Figure 2). For fullspan laminar flow models, the common strategy is to put all the leading-edge pressure ports on one wing and use the other wing to observe the laminar flow. However, that strategy is not feasible for semispan models, so the two layout system was devised. To avoid loss of laminar flow at every pressure port row, Layout A was only used on 4 of the 9 rows (seen in Figure 13). The orifice diameters of the pressure ports were also reduced near the leading edge to 0.010 inches; all ports aft of x/c = 0.25 and on the lower surface had an orifice diameter of 0.020 inches.

In addition to static pressure ports, the wing was instrumented with 18-gauge wires that were routed internally through the model to specific locations on the surface. These wires were used to pass an electric current for the transition visualization technique that is described in the following subsection. Routing the wires internally in the model eliminated the need to secure the wiring to the model surface as was done during previous testing using this technique. The wires exit the internal channels and reach the surface at 4 locations on the upper surface (as visualized in Figure 13) and 4 similar locations on the lower surface. The computational design and analysis assumed a fully-turbulent lower surface of the wing, so trip dots were added to the lower surface of the model to ensure a turbulent boundary layer. Trip dots were also added to the nose of the fuselage.

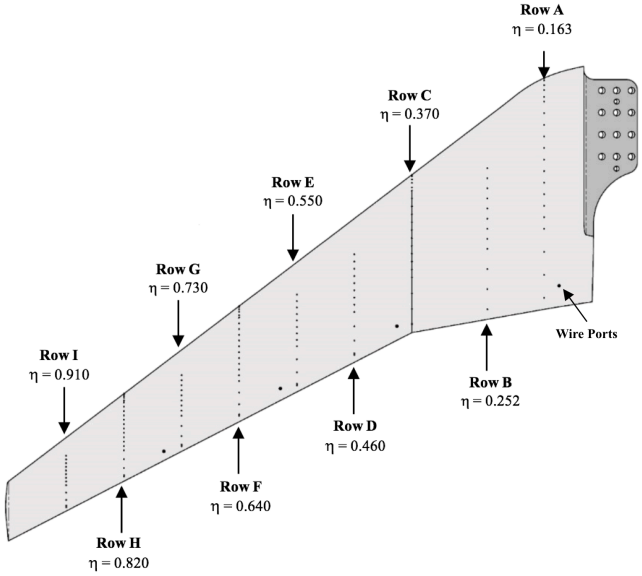

Figure 13. Planform view of the CRM-NLF wing semispan model. The 9 pressure port rows are labeled and show the upper surface pressure orifice distribution. The location of the 4 upper surface wire ports are shown as black circles near the trailing edge.

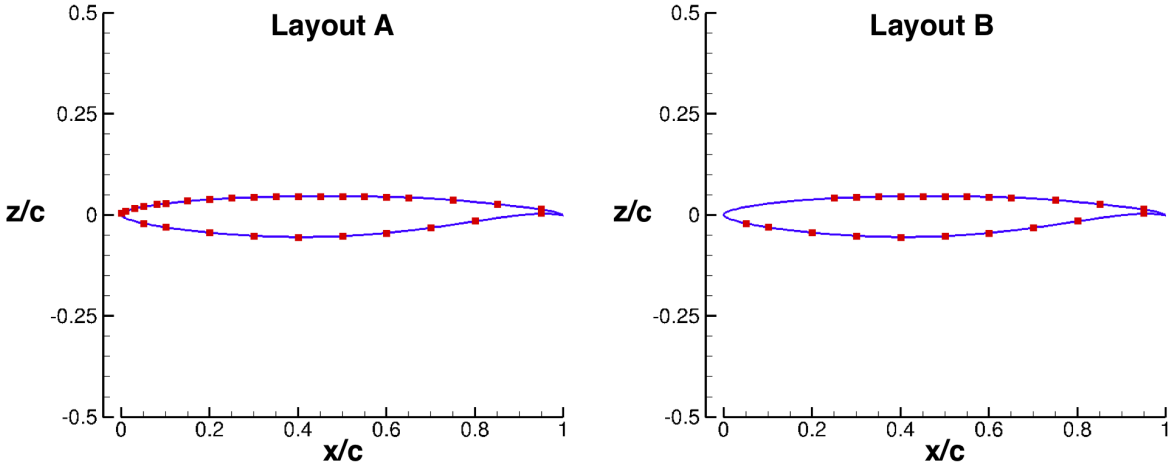

Figure 14. Example of the distribution of static pressure ports for Layout A (left) and Layout B (right). The two layouts only differ in the leading-edge region of the upper surface.

During the test, several types of data were acquired to help evaluate the three main test goals, including force and moment, static pressure, model deformation, and transition visualization data. The force and moment data were obtained using the NTF-117S force and moment strain gauge balance via the NTF external Force Measurement System (FMS) inside the Sidewall Model Support System (SMSS). The force and moment data technique replicated a previously successful semispan test, which has a more detailed description of this NTF semispan measurement system in the test report [23]. The wing and fuselage pressures were measured using 6 Electronically Scanned Pressure (ESP) modules located inside the model. The data obtained through the tunnel data acquisition system were collected at 80 Hz over either 8- or 30-second periods, depending on the type of transition visualization technique being used. The data obtained at steady-state conditions were conditionally sampled to improve the accuracy of the data and determine the nominal condition at each point. The data obtained during a rapid liquid nitrogen injection, which were used for the transition visualization technique, was averaged to determine the nominal condition. All data in this report are uncorrected for tunnel wall effects. Model deformation data were obtained at the end of the test using a Video Measurement System (VMS). The VMS uses an array of cameras and targets applied to the upper surface of the wing to calculate the wing twist and deflection under various loading conditions.

The majority of data was acquired near the design cruise condition. At the beginning of the test, larger polars (angles of attack of 0 to 8 deg.) were run at near-cruise Mach numbers (0.84, 0.85, and 0.86) to determine the condition that most closely matched the computational design point. The Mach 0.86 test condition provided the best agreement to computational predictions of Mach 0.85, so the remainder of the test was conducted at this speed. Table 2 provides a summary of the approximated primary test conditions where the majority of data was acquired. Additional detail on the agreement between experimental and computational results is provided in the following section.

Table 2. Summary of the approximated primary test conditions.

Primary Test Conditions						
Mach	**α (deg.)**	**T_t (°F)**	**P_t (psia)**	**q_∞ (psfa)**	**Re_{ft} (x10^6)**	**Re_{MAC} (x10^6)**
0.86	1.5 to 3.0	+40	26 to 39	1180 to 1780	8.4 to 12.6	10.0 to 15.0
		-50	24 to 39	1120 to 1800	10.5 to 16.7	12.5 to 20.0
		-150	26 to 39	1200 to 1800	16.7 to 25.1	20.0 to 30.0

For the purpose of evaluating the CATNLF design method, the surface static pressure data and transition visualization data are most valuable, so this report will focus primarily on analyzing these results. The following subsection describes the transition visualization techniques used during the test. Some force and moment results are included in the companion paper [8].

C. Transition Visualization Techniques

The transition visualization data acquired during the test were obtained using temperature sensitive paint (TSP) [24]. This paint enables images to be taken that show temperature differences on the surface. Laminar flow on an aerodynamic surface can be visualized using this technique due to the heat transfer difference between laminar and turbulent boundary layers. When a temperature gradient is introduced to the system, a turbulent boundary layer will transfer heat faster than a laminar boundary layer, and a TSP image can be taken that shows this temperature difference on the surface. This transition visualization technique is used for cryogenic testing in which traditional infrared (IR) thermography or sublimating chemicals is more difficult to implement. At the NTF, the required temperature gradient is typically introduced via a rapid injection of liquid nitrogen. This method successfully produces the necessary temperature gradient for TSP images, although it alters the tunnel conditions during data acquisition and increases the total cost and consumption of liquid nitrogen. To alleviate these adverse effects, recent work has been conducted to develop an alternate method of producing the temperature gradient via a carbon-based resistive heating layer [25,26]. This carbon-based resistive heating layer is applied beneath the TSP and is connected to electrical leads that provide current to heat the model surface. Details on the painting technique and the various layers needed for this carbon-based resistive heating layer to function are provided in a paper by Watkins et al. titled "Transition Detection at Cryogenic Temperatures Using a Carbon-Based Resistive Heating Layer Coupled with Temperature Sensitive Paint" [27].

The CRM-NLF model was painted twice during the wind tunnel test. After the first month of acquiring data, the test was paused to make tunnel repairs. During this pause in testing, the wing was removed from the test section for repainting to make improvements to the heating layer and overall surface finish. The portion of the test prior to tunnel repairs is referred to as Phase 1, and the portion after the tunnel repairs as Phase 2. The majority of the data was collected during Phase 2. For Phase 1, the carbon-based resistive heating layer was applied with constant resistance over the entire wing span. Due to the significant surface area and thickness difference between the wing root and tip, the Phase 1 heating layer only provided enough of a temperature gradient to visualize transition on the outboard half of the wing. The temperature gradient was also reduced by the higher resistance of the coating, which limited the amount of power that could be applied to the wing. In an effort to provide even heating across the span of the wing, the carbon-based resistive heating layer was applied with spatially variable resistance for Phase 2. The inboard portion of the wing, where the surface area and thickness are much larger, had lower resistance compared to the outboard portion of the wing. The lower resistance areas inboard would heat faster, providing a more even temperature gradient across the span of the wing. This spatial resistance difference was enabled by switching the carbon-content from the carbon black used in Phase 1 to graphite in Phase 2. Graphite has a lower overall resistance and could therefore be used more easily to provide different resistance zones on the wing, as well as allow more power to be delivered. The content of graphite in the layer was spatially altered in such a way that the layer was as even as possible and had a higher concentration of graphite inboard than outboard (as graphite concentration increases, resistance decreases). The paint application method for Phase 2 provided sufficient temperature gradient to visualize transition across the span of the wing using the heating layer.

Laminar flow is highly dependent on surface quality. Wind tunnel model size limitations often mean the boundary layers are thin at the unit Reynolds numbers required to mimic flight conditions. These thin boundary layers are extremely sensitive to any surface imperfections, such as particulates in the tunnel, oil, ice crystals, or surface defects caused by a particle impact. A laminar boundary layer that encounters any of these surface imperfections can transition if the imperfection is of critical height, creating a turbulent wedge emanating from the imperfection. The critical height is a function of the boundary layer thickness, so as the Reynolds number increases and the boundary layer thins, surface imperfections of a fixed size will increasingly become critical. This results in more turbulent wedges seen at higher Reynolds numbers. While the NTF maintains very high standards for cleanliness during any test, laminar flow testing is exceptionally sensitive to any contaminants. Therefore, the NTF undergoes additional cleaning and contamination-prevention procedures during a laminar flow test to minimize the potential of introducing any contaminants into the tunnel. In addition to these procedures, the top coat of paint on the model was sanded and polished frequently during the test. This sanding and polishing allowed the data to be collected with the best-possible surface quality, and a visible reduction in turbulent wedges was seen each time the paint was sanded and polished. Table 3 provides the thickness and roughness measurements of the paint in Phase 2. This table shows that the overall thickness and roughness of the paint was reduced by the additional sanding and polishing that occurred during testing.

Table 3. Thickness and roughness measurements of the Phase 2 paint application as measured before and after Phase 2 testing.

Phase 2 Paint Surface Characteristics			
Measurement	**Location**	**Average Value Prior to Testing**	**Average Value After Testing**
Thickness	Inboard	16.35 mils	15.48 mils
	Midspan	12.15 mils	11.80 mils
	Outboard	10.83 mils	10.62 mils
Roughness	Leading Edge	1.64 µin	1.10 µin
	50% Chord	0.90 µin	0.83 µin

Throughout the test, TSP images were acquired at each condition using both the rapid liquid nitrogen injection method and the carbon-based resistive heating layer method. This enables direct comparison of the two methods in hopes of establishing best practices for future laminar flow tests using TSP images. A comparison of the two temperature gradient methods can be seen in Figures 15 and 16. The TSP image from each method at the same test condition is shown in Figure 15, and two relevant tunnel conditions during the data collection from each method is shown in Figure 16. The additional turbulent wedges seen in the TSP image using the rapid liquid nitrogen injection method is not necessarily a result of the temperature step mechanism, but could be a consequence of the number of data points taken between the two images. Turbulent wedges accumulated steadily during testing, and only were reduced when the wing was sanded and polished. The heating layer images were acquired prior to the liquid nitrogen injection images, so often the heating layer images showed fewer turbulent wedges. For the TSP images from the rapid liquid nitrogen injection method, the scales were adjusted so that laminar flow is depicted as lighter color regions. The tunnel conditions comparison in Figure 16 highlights the added stability of tunnel conditions when using the new carbon-based heating layer. The impact of the stability of tunnel conditions on the transition front can be seen when looking at frame-by-frame TSP images. Prior to advanced post-processing of the images, the rapid liquid nitrogen injection method did often provide images with higher contrast, which gave a more clear distinction between the laminar and turbulent regions on the wing during the test. However, with the advanced post-processing techniques performed after the test, the heating layer images had sufficient contrast to allow for laminar flow analysis. Based on the data collected during the test, the carbon-based heating layer from Phase 2 was the preferred method for acquiring transition visualization images. The following section will provide a sample of pressure data, TSP images, and preliminary analysis in support of the test goal to validate the CATNLF design method and computational tools.

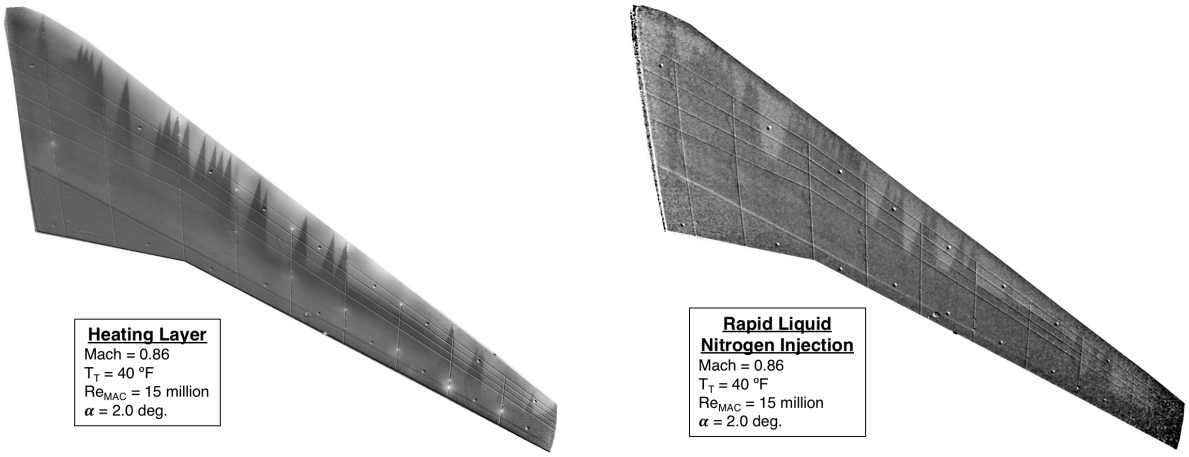

Figure 15. TSP images using the two temperature gradient methods: the heating layer (left) and the rapid liquid nitrogen injection (right). Both images were taken at M = 0.86, T_T = 40 °F, α = 2 deg., and Re_{MAC} = 15 million.

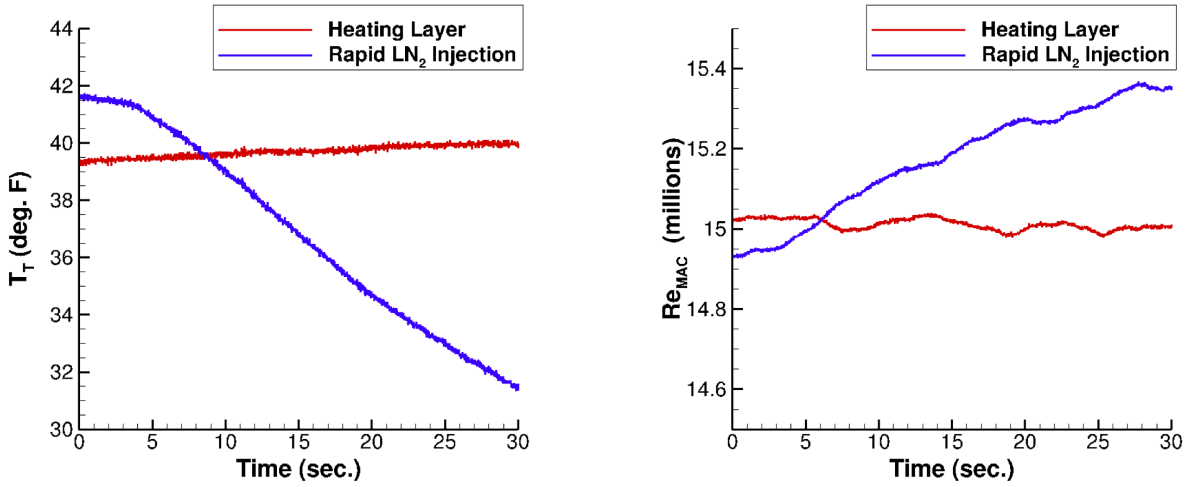

a) Total temperature versus time.

b) Reynolds number versus time.

Figure 16. Changes in total temperature (T_T) and mean aerodynamic chord Reynolds number (Re_{MAC}) during the 30 second data points using the heating layer method (red line) and the rapid liquid nitrogen injection method (blue line). The data correspond to the two TSP images in Figure 15 at M = 0.86, T_T = 40 °F, α = 2 deg., and Re_{MAC} = 15 million.

IV. Results and Discussions

The experimental investigation of the CRM-NLF model in the NTF had 3 primary test goals as listed in the Introduction section. In this report, preliminary results will be presented to begin evaluating the first goal of validating the CATNLF design method and computational tools. The primary test data needed for this assessment are pressure data and TSP images. The section will offer initial findings and discussions regarding the experimental assessment of the CATNLF design method.

A. Comparison of Computational and Experimental Surface Pressures

Surface pressures are essential for the validation of the CATNLF design method and computational tools. The CATNLF design method uses pressure gradients to delay transition, and the boundary layer and stability analysis software uses pressure distributions to estimate transition location. Adequate pressure matching between the CFD and experimental data is essential to be able to use the stability analysis software to analyze the TSP images.

The data from the 9 rows of static pressure ports are used to determine the wind tunnel conditions that provided the best agreement to the CFD data. Upon comparing the CFD and experimental pressure distributions at a variety of wind tunnel conditions, it was determined that the best agreement between pressures occurred with a Mach shift of 0.01 according to Equation 1.

$$M_{CFD} = M_{WT} - 0.01 \tag{1}$$

This Mach shift was identified at the early stages of the wind tunnel test, so the majority of the experimental data were acquired at Mach 0.86 to correspond to the computational design condition of Mach 0.85, as noted in Table 2. The direction of the Mach shift (wind tunnel higher than CFD) is consistent with previous semispan testing in the NTF [23]. The wind tunnel pressure data in this report are scaled according to this Mach shift.

In addition to the Mach shift, an adjustment to the angle of attack was needed to provide the best agreement between CFD and wind tunnel conditions. The angle-of-attack shift was dependent on the wing deflection and was a function of the dynamic pressure used during data acquisition and the experimental angle of attack. As the dynamic pressure was altered to test at different Reynolds numbers, the deflection of the model changed. At lower dynamic pressures, the wingtip twist was reduced compared to the higher dynamic pressures. Additionally, the experimental angle of attack altered the wingtip twist deflection, with higher experimental angles of attack resulting in higher wingtip twist. There is also uncertainty in the magnitude and spatial variation of the tunnel flow angularity, which may cause a spanwise variation in angle-of-attack shift. These factors led to spanwise variation of the angle-of-attack

shift needed to correlate the experimental data to the CFD results. For the analyses in this report, the angle-of-attack shift is applied by matching each of the 9 pressure port rows individually to CFD solutions. In the initial results contained in this report, the maximum angle-of-attack shift needed was 0.25 degrees. For future analyses, the VMS model deflection data will be used to quantify the wing twist changes that occurred with changing dynamic pressure and angle of attack. Two examples of the pressure data correlation seen between wind tunnel data (scaled for the Mach shift as previously described) and CFD are shown in Figures 17 and 18. The example pressure rows and angles of attack shown in the figures are representative of the agreement seen in the data collected. In general, the agreement between wind tunnel and CFD pressures was very good, suggesting the general characteristics needed for the CATNLF method were obtained on the wind tunnel model. The rows with pressure ports near the leading edge show the rapid acceleration used for crossflow attenuation.

As mentioned previously, the boundary layer and stability analysis software use surface pressure distributions to estimate transition location. It is desirable to use the acquired wind tunnel pressure data in these computations to analyze the TSP transition images from the test. However, the practical limitation of installing pressure orifices in the model, especially near the wing leading edge, means that the distribution of data will be fairly coarse, even for the larger scale afforded by the semispan model. In an effort to retain the true character of the experimental pressure distribution, the procedure for infilling the pressures between orifice locations utilized results from CFD. In this procedure, the difference between the wind tunnel and CFD pressure at each orifice location is computed. This array of differences is linearly interpolated to the CFD pressure locations and added to the pressure values. The differences ahead of the first point on the upper surface for full-chord orifice rows (Layout A, first port at $x/c = 0.001$) were linearly scaled to zero at the leading edge. For the stations where the first orifice on the upper surface was further aft (Layout B, first port at $x/c = 0.25$), the pressure difference at the first orifice was held constant forward until $x/c = 0.001$, where it was linearly tapered to zero. This means that for these Layout B pressure distributions, the infilled experimental data match the CFD forward of $x/c = 0.25$, as there is no experimental information in this region. The lower surface pressures near the leading edge were treated similarly such that the pressures near the attachment line matched the CFD. Finally, the resulting pressure distributions were smoothed to remove spurious variation while retaining the basic character of the distribution. The results of this infilling technique can be seen in Figures 19 and 20 labeled as “Infilled WT”. The infilled experimental data will be used for the boundary layer and stability analysis computations presented in this report.

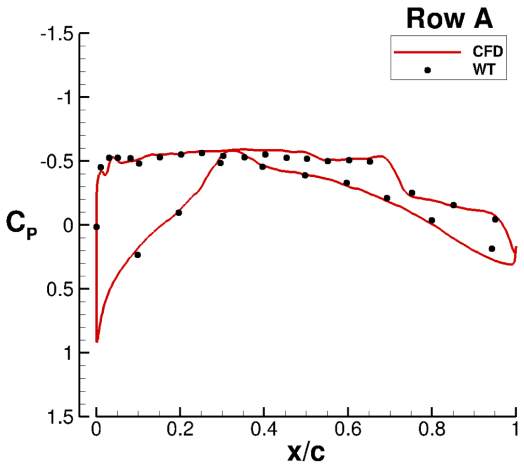

a) Pressure distribution for Row A.

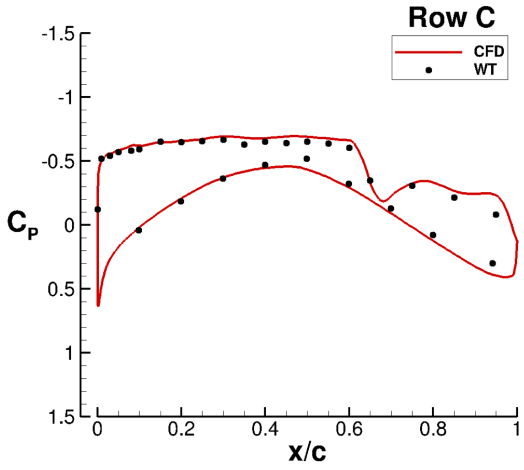

b) Pressure distribution for Row C.

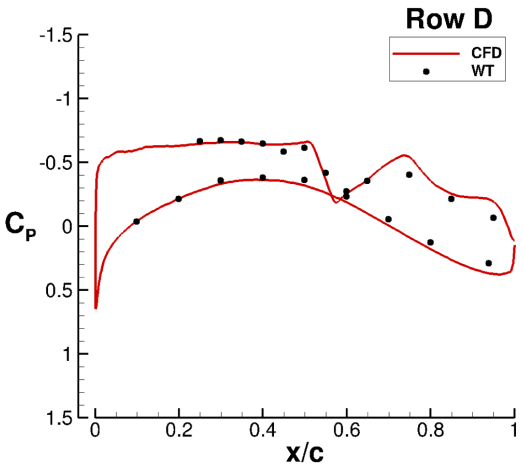

c) Pressure distribution for Row D.

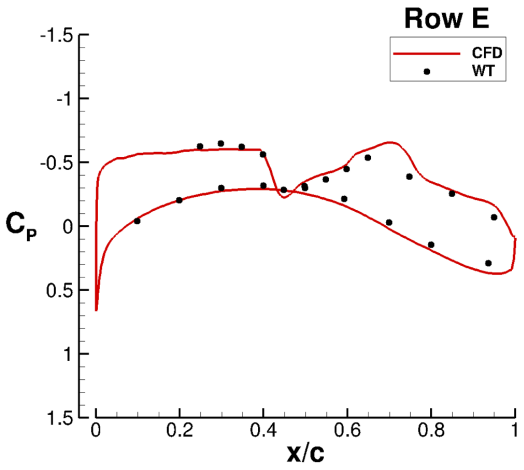

d) Pressure distribution for Row E.

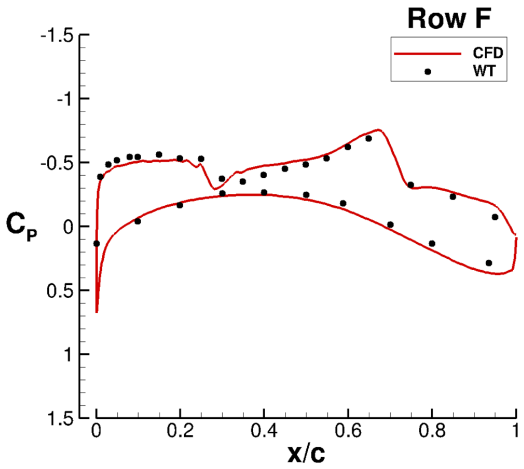

e) Pressure distribution for Row F.

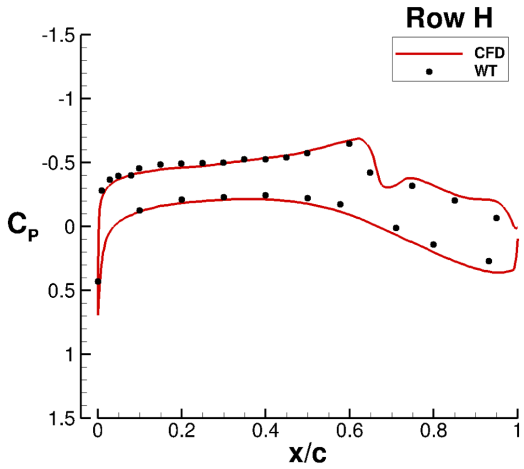

f) Pressure distribution for Row H.

Figure 17. Example correlation between wind tunnel pressures ("WT", black circles) and computational results ("CFD", red line). The Mach and angle-of-attack shifts have been applied. The experimental conditions are M = 0.86, T_T = 40 °F, α = 1.5 deg., and Re_{MAC} = 15 million.

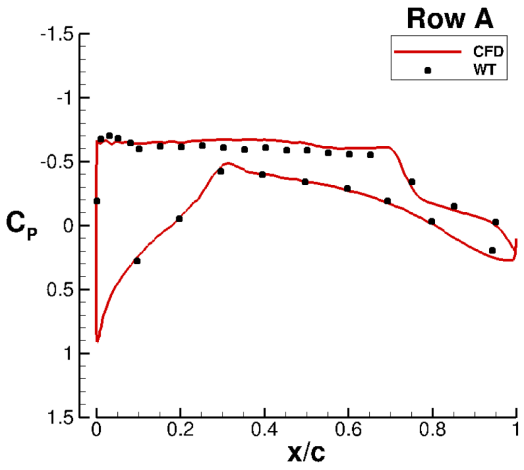

a) Pressure distribution for Row A.

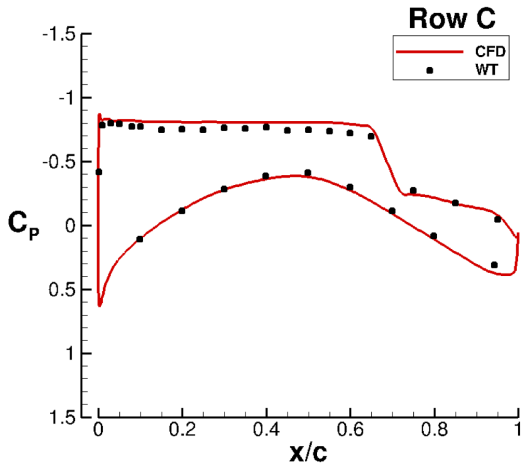

b) Pressure distribution for Row C.

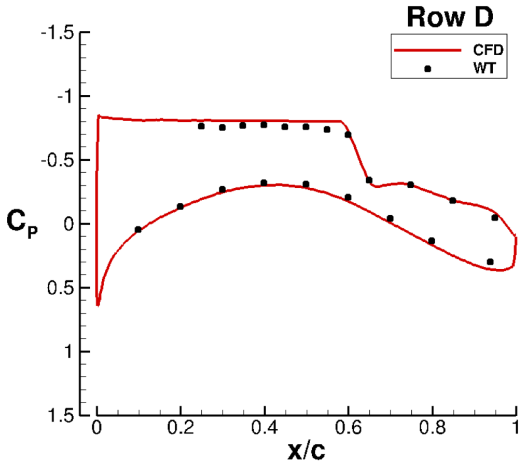

c) Pressure distribution for Row D.

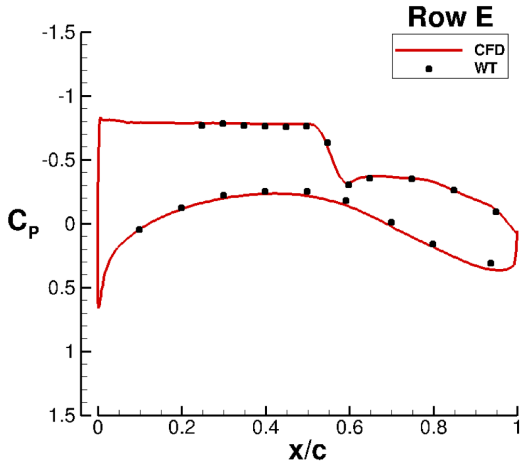

d) Pressure distribution for Row E.

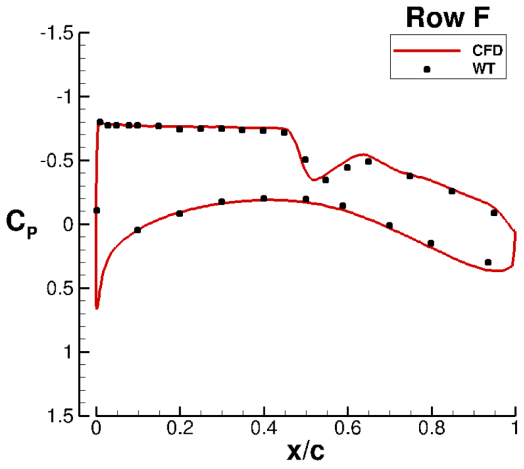

e) Pressure distribution for Row F.

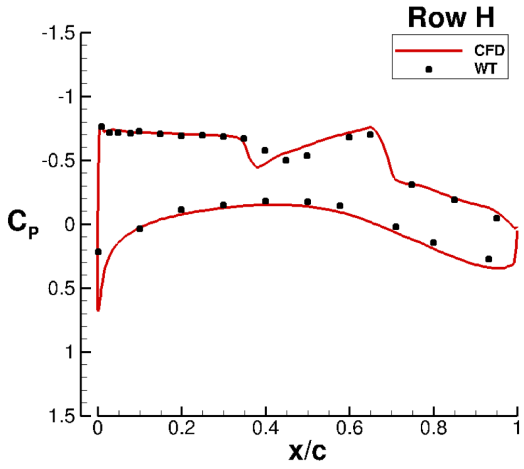

f) Pressure distribution for Row H.

Figure 18. Example correlation between wind tunnel pressures ("WT", black circles) and computational results ("CFD", red line). The Mach and angle-of-attack shifts have been applied. The experimental conditions are M = 0.86, T_T = 40 °F, α = 2.5 deg., and Re_{MAC} = 15 million.

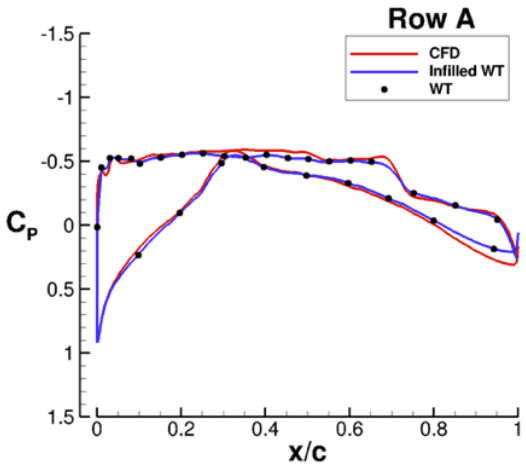

a) Pressure distribution for Row A.

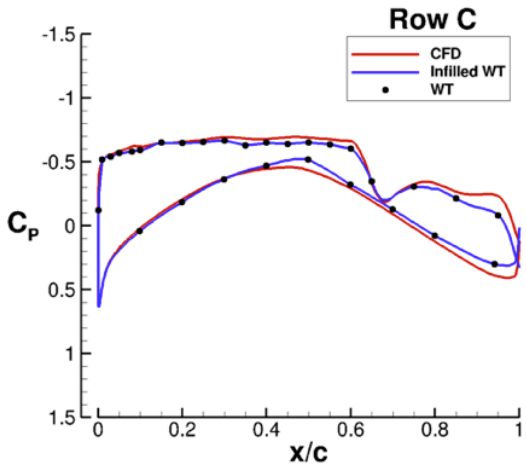

b) Pressure distribution for Row C.

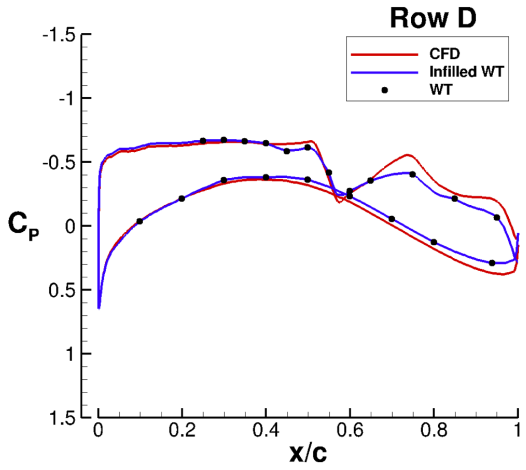

c) Pressure distribution for Row D.

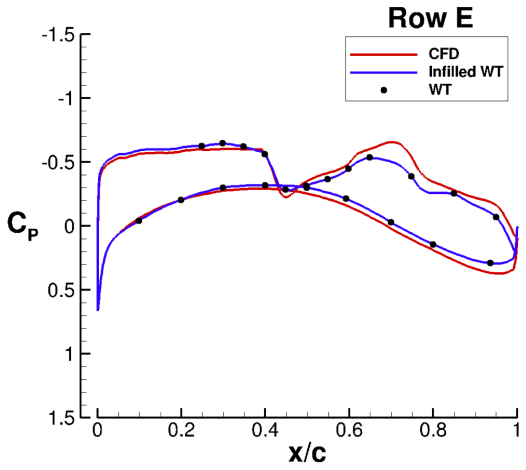

d) Pressure distribution for Row E.

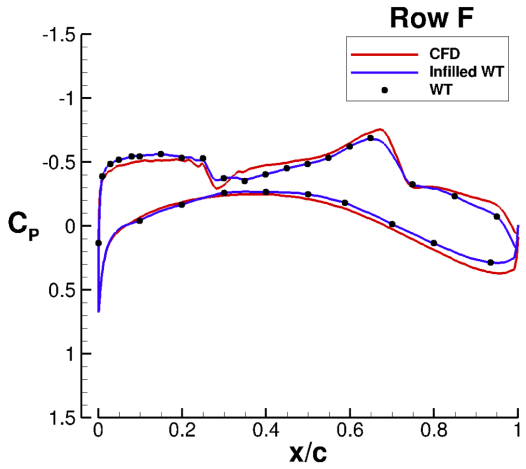

e) Pressure distribution for Row F.

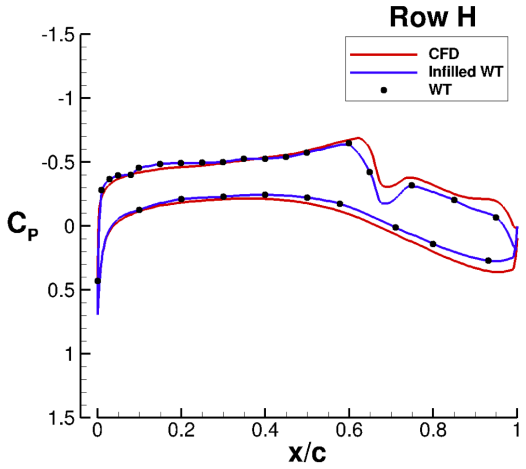

f) Pressure distribution for Row H.

Figure 19. Example of how the infilled wind tunnel pressures ("Infilled WT", blue line) compare with the CFD and wind tunnel (WT) data from Figure 17. The infilled wind tunnel pressures are used for stability analysis and transition prediction. The experimental conditions are M = 0.86, T_T = 40 °F, α = 1.5 deg., and Re_{MAC} = 15 million.

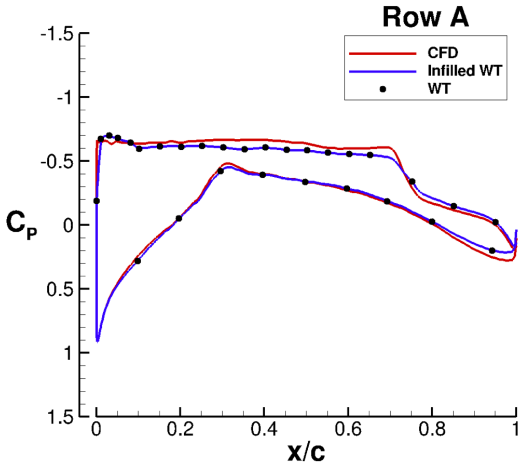

a) Pressure distribution for Row A.

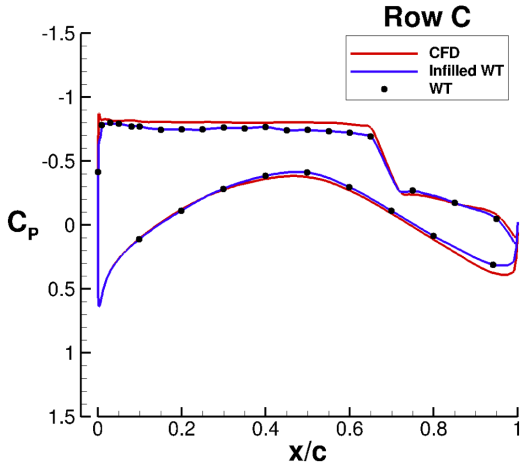

b) Pressure distribution for Row C.

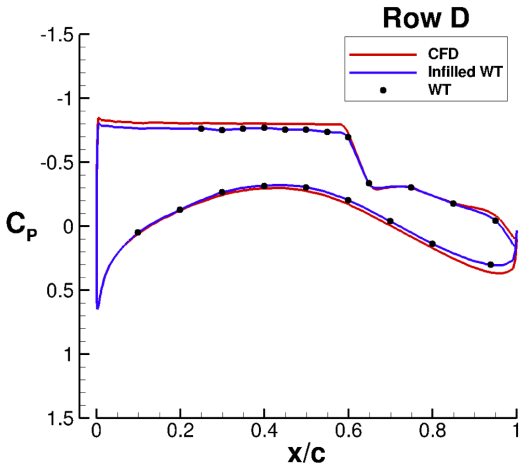

c) Pressure distribution for Row D.

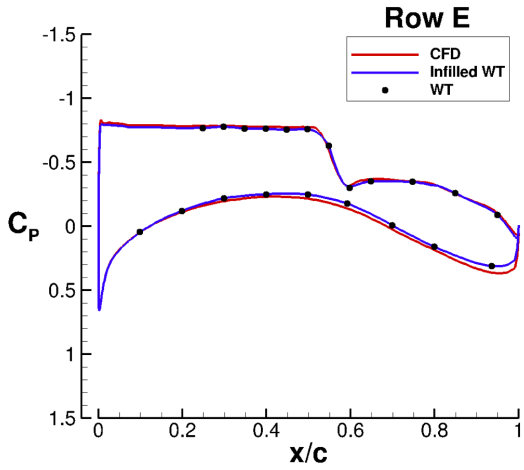

d) Pressure distribution for Row E.

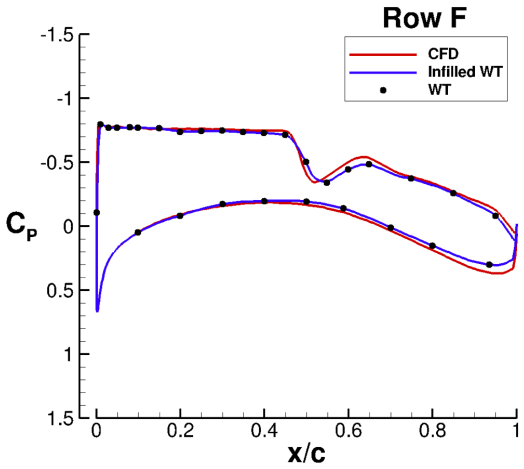

e) Pressure distribution for Row F.

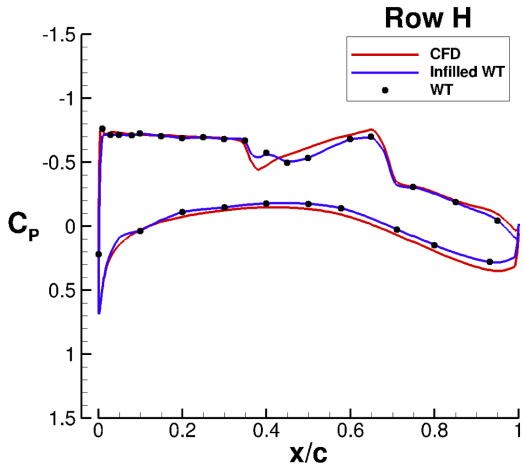

f) Pressure distribution for Row H.

Figure 20. Example of how the infilled wind tunnel pressures ("Infilled WT", blue line) compare with the CFD and wind tunnel (WT) data from Figure 18. The infilled wind tunnel pressures are used for stability analysis and transition prediction. The experimental conditions are M = 0.86, T_T = 40 °F, α = 2.5 deg., and Re_{MAC} = 15 million.

B. Analysis of Transition Delay Using CATNLF Method

The primary purpose of this report is to provide a preliminary assessment of the new CATNLF method. The transition front images acquired during the test are analyzed in an attempt to draw conclusions on the effectiveness of the method to delay transition. This section will provide a sample of transition images at a variety of conditions, as well as a discussion on attachment line transition and transition due to crossflow and Tollmien-Schlichting.

1. Sample Transition Images

The transition images acquired during the experiment in the NTF are the primary source of information on the effectiveness of the CATNLF method in delaying transition. To properly evaluate the CATNLF method, a series of images over a range of conditions are needed that show the transition front across the wing. These transition fronts are compared against computational predictions of crossflow and Tollmien-Schlichting growth, as well as attachment line Re_θ values when relevant. One major challenge with using these experimental transition images is that bypass transition is often visible in the images, and that can make it difficult to determine the natural transition front (i.e., not bypass-related) at a given condition. This bypass transition is typically caused by very small surface imperfections (particulates in the tunnel, paint damage, etc.) and mandates sanding and polishing the surface to remove the imperfection. The bypass transition appears in the image as a turbulent wedge emanating from the imperfection and, if the wedges become too frequent, these wedges can coalesce ahead of the natural transition front such that no front can be determined. This becomes a more common issue at the higher Reynolds number conditions where the boundary layer is thinner. During this experiment, repeating test points was vital to ensure the best possible image was acquired at a given condition. Figure 21 shows a sample of repeat points acquired throughout the test at a single condition. The wide range in quality of the images highlights the challenges associated with laminar flow wind tunnel tests. The gridlines seen in the images were drawn on the model to help determine extent of laminar flow. The spanwise lines correspond to 20, 30, 40, and 50% local chord, and the chordwise lines are where the 9 pressure port rows are located.

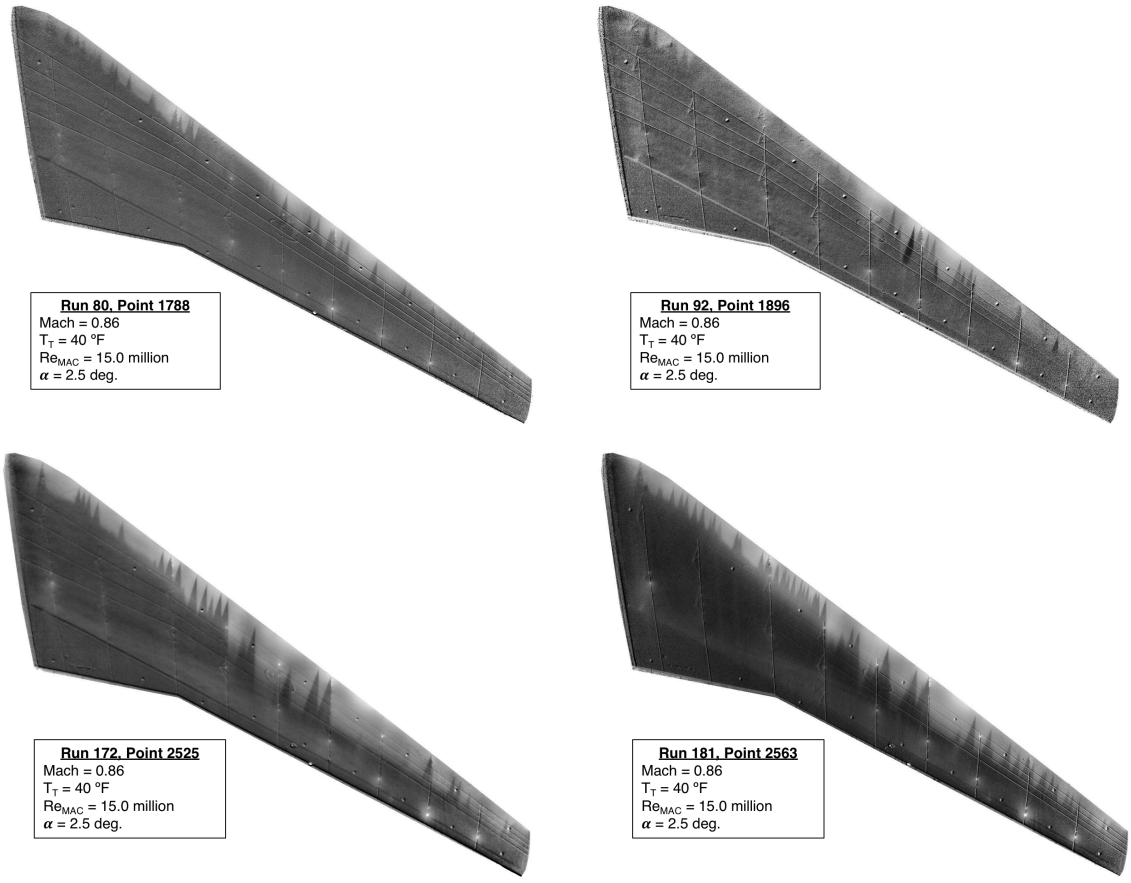

Figure 21. Example of variety in TSP images from repeat points. All images use the heating layer method and were acquired at tunnel conditions of M = 0.86, T_T=40 °F, α = 2.5 deg., and Re_{MAC} = 15 million.

The objective for this test was to acquire a series of good quality images showing the progression of laminar flow at a range of conditions. The primary focus was on near-cruise angles of attack at a variety of Reynolds numbers. A sample series of images from the 4 main angles of attack is shown in Figure 22. The varying extents of laminar flow with angle of attack can clearly be seen inboard, where the higher angles transition much further forward than the lower angles. Additionally, an example of the Reynolds number effect on laminar flow extent can be seen in the series of images found in Figure 23. The images in this figure, ranging from Reynolds numbers based on mean aerodynamic chord of 10 – 22.5 million, illustrate the challenges with high Reynolds number testing due to the significant increase in turbulent wedges from bypass transition. TSP images were also acquired at Reynolds numbers based on mean aerodynamic chord of 25, 27.5, and 30 million, each showing small regions of laminar flow inboard and outboard. However, due to the increase in turbulent wedges, the higher Reynolds number images are used less for the evaluation of the CATNLF method.

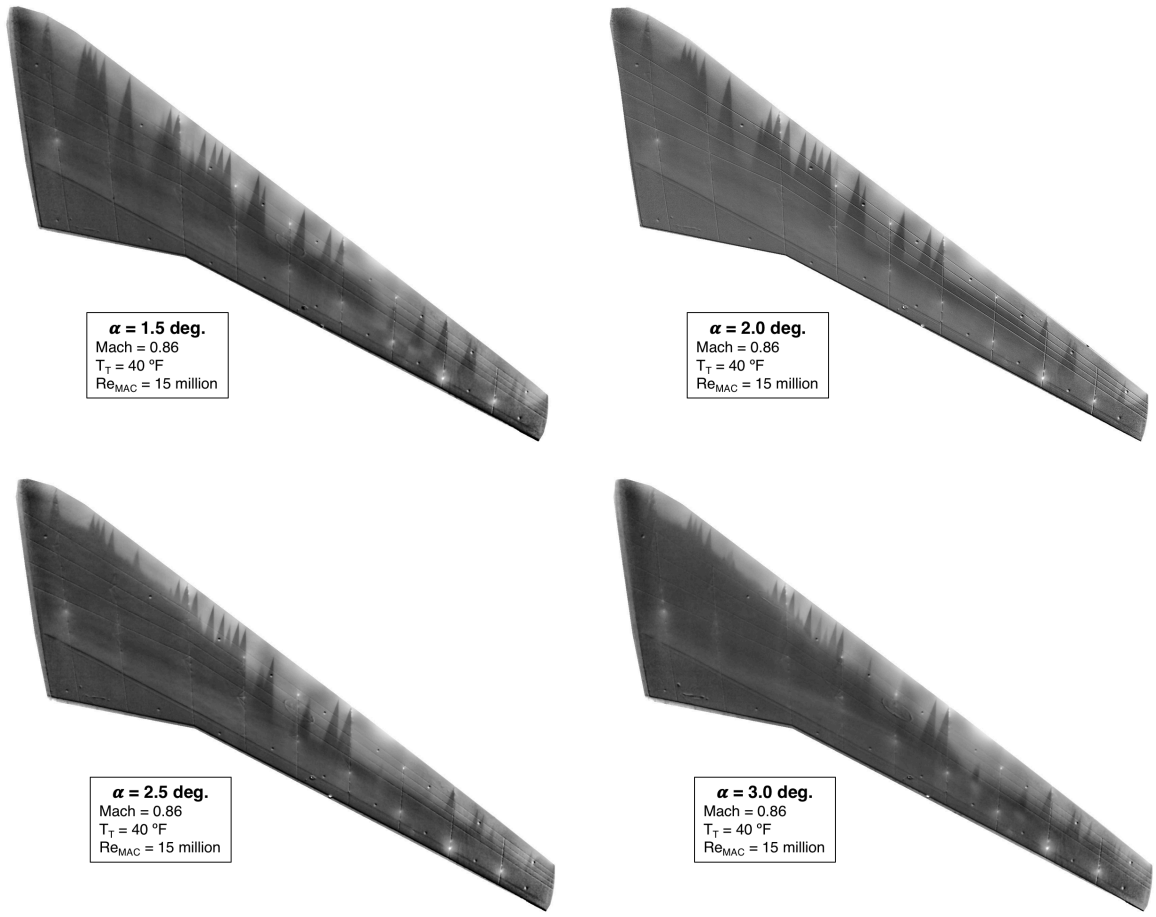

Figure 22. Example of TSP images from an angle-of-attack sweep. All images use the heating layer method and were acquired at the tunnel conditions of M=0.86, T_T=40 °F, and Re_{MAC}=15 million.

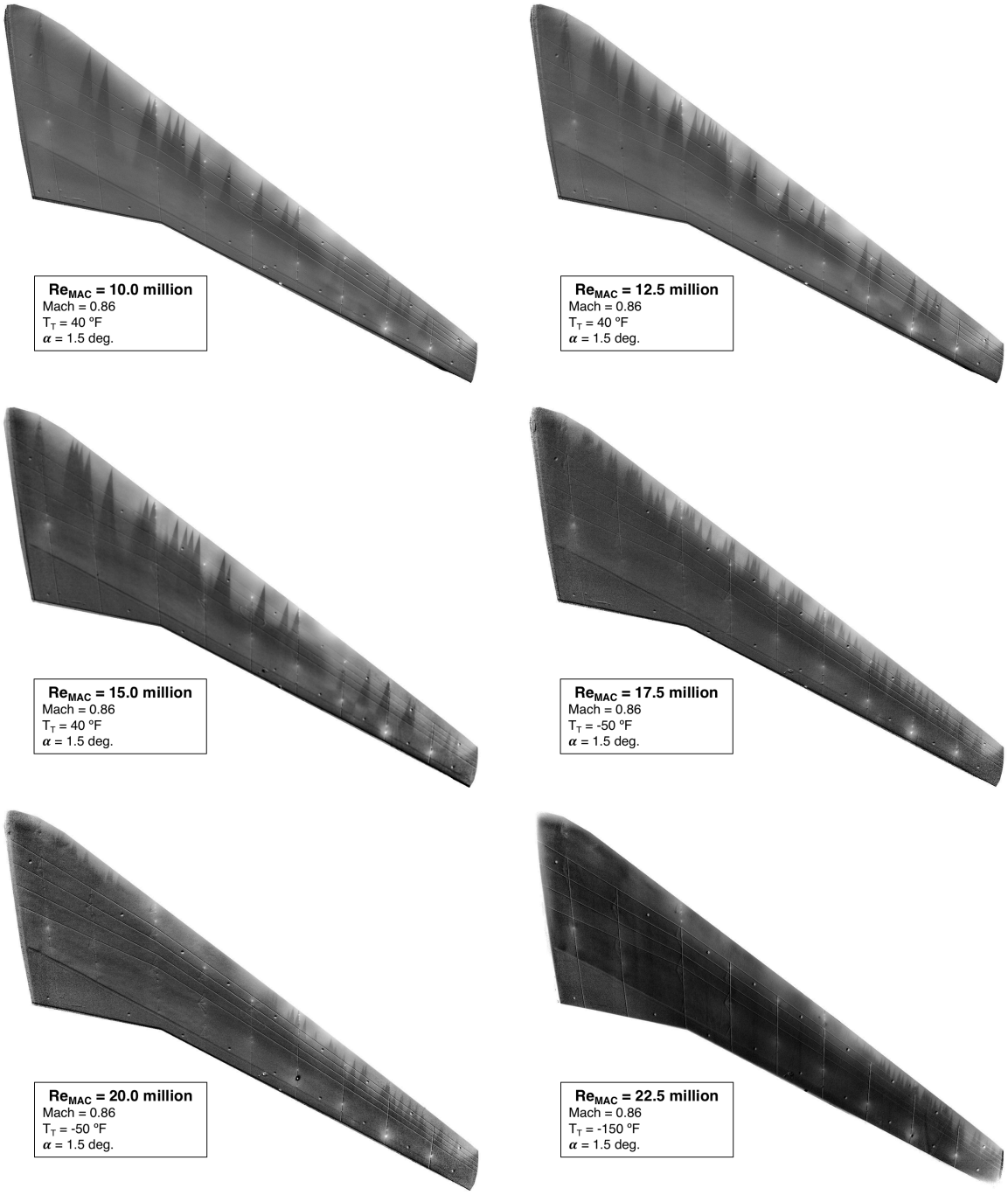

Figure 23. Example of TSP images from a Reynolds number sweep. All images use the heating layer method and were acquired at the tunnel conditions of M=0.86 and α=1.5 deg. The frequency of turbulent wedges increases with Reynolds number. Data were also acquired at 25, 27.5 and 30 million Reynolds number, showing increasingly small regions of laminar flow at each condition.

2. Attachment Line Transition

The strategy employed in this test to guard against attachment line contamination and transition was previously presented in the Model Design subsection. As mentioned above, only a small portion of the span inboard and outboard had attachment line Re_θ values low enough to relaminarize the boundary layer according to Poll's criteria (i.e., Re_θ values less than 100). The majority of the wing had Re_θ values between 100 and 235, suggesting that the state of the boundary layer would depend on the inboard boundary layer. The intent was that the low Re_θ values on the reduced sweep section inboard would relaminarize the turbulent boundary layer from the fuselage creating a laminar boundary layer traveling outboard along the wing. Then the Re_θ requirement could be relaxed to the 235 limit and the boundary layer would remain laminar across the span of the wing. This strategy proved to work well to eliminate attachment line contamination and transition (transition caused by high Re_θ values), but did not offer any protection against attachment line bypass transition. If bypass transition due to a surface imperfection occurred on the attachment line past the reduced sweep section inboard, the attachment line would remain turbulent until the Re_θ values returned below the relaminarization limit of 100. Once the attachment line is turbulent, all chordwise laminar flow is lost until the attachment line is relaminarized. In the images, this attachment line transition appeared as leading-edge transition across the midspan region of the wing, with pockets of laminar flow visible inboard and outboard where the Re_θ values are sufficiently low. One unique challenge with attachment line transition is its visual similarity to crossflow transition, which often also appears as leading-edge transition on swept wings at higher Reynolds numbers. The primary way to experimentally determine if the leading-edge transition was due to a turbulent attachment line was to take repeat images. If any image showed no leading-edge transition across the span, or if the spanwise relaminarization location changed significantly between images, it could be inferred the transition was due to bypass transition of the attachment line. Figure 24 shows one example of a pair of images from the same test conditions; the image on the left shows full-span laminar flow, and the image on the right shows midspan leading-edge transition. Seeing full-span laminar flow in one image suggests that the leading-edge transition is caused by attachment line bypass transition. On the image with leading-edge transition, two markers are shown corresponding to the beginning and the end of leading-edge transition. The corresponding Re_θ values for the image shown can be seen in Figure 25. The two markers indicating the spanwise location of the beginning and end of the leading-edge transition are shown on the plot. It can be seen that the leading-edge transition begins in a region where the Re_θ values are above the laminar boundary of 100. The leading-edge transition ends once the Re_θ values fall below 100. For this example, the Re_θ value at relaminarization was approximately 100. Figure 26 shows another example pair of images from a different angle of attack and Reynolds number, indicating attachment line bypass transition. Similar markings can be seen on the right image corresponding to the beginning and end of leading-edge transition. The Re_θ values from this condition are plotted in Figure 27, showing again that the leading-edge transition begins in a region where Re_θ is greater than 100 and ends once the Re_θ falls below 100 outboard. The Re_θ value at relaminarization in this example was approximately 98.

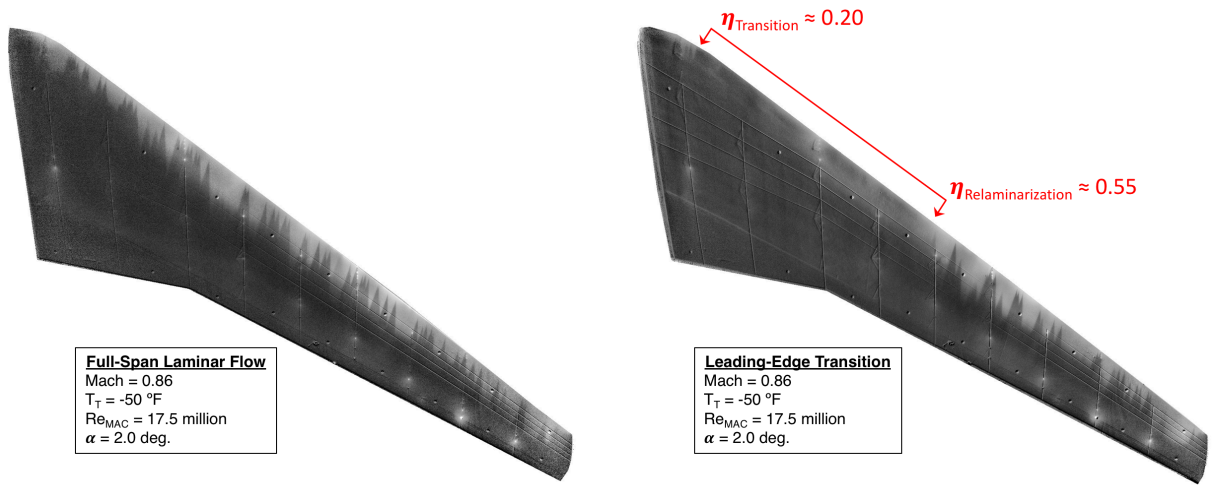

Figure 24. Two TSP images from the same test conditions of M = 0.86, T_T = -50 °F, α = 2.0 deg., and Re_{MAC} = 17.5 million, one showing full-span laminar flow (left) and one showing leading-edge transition (right). The image with leading-edge transition has approximate semispan locations for when transition and relaminarization occur.

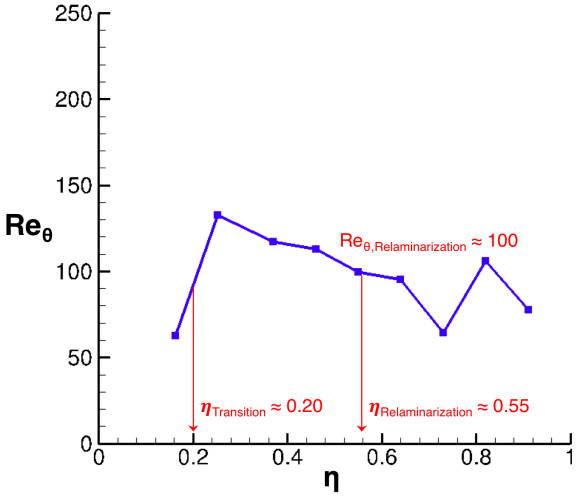

Figure 25. Spanwise distribution of attachment line Re_θ values for the TSP image with leading-edge transition from Figure 24 (M = 0.86, T_T = -50 °F, α = 2.0 deg., and Re_{MAC} = 17.5 million). Markers showing the approximate semispan location of transition and relaminarization are shown. The Re_θ value at relaminarization is approximately 100.

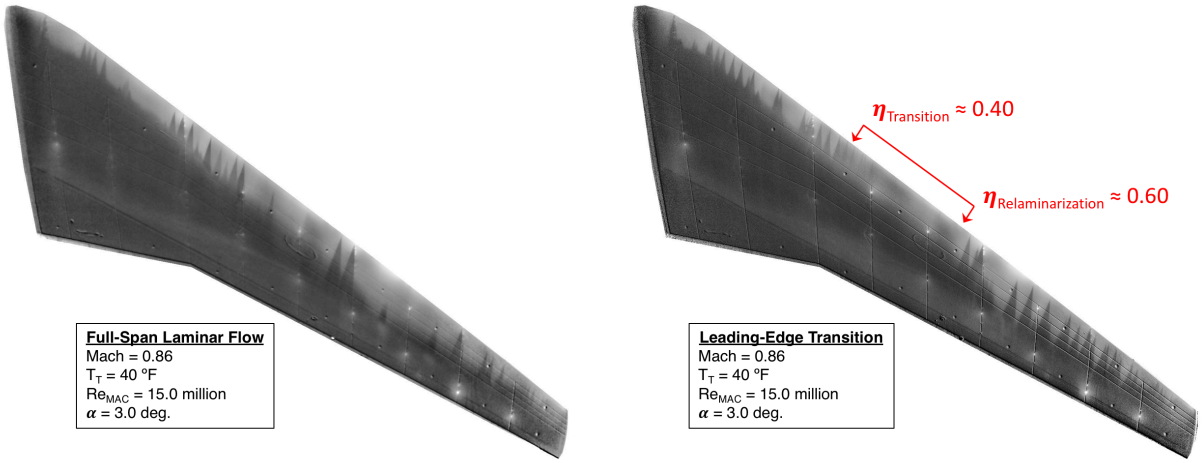

Figure 26. Two TSP images from the same test conditions of M = 0.86, T_T = 40 °F, α = 3.0 deg., and Re_{MAC} = 15.0 million, one showing full-span laminar flow (left) and one showing leading-edge transition (right). The image with leading-edge transition has approximate semispan locations for when transition and relaminarization occur.

The transition images acquired during this test helped experimentally validate the design strategy used to guard against transition caused by a turbulent attachment line, as well as validate the computational tool used to calculate attachment line Re_θ values. The images showing attachment line bypass transition were uniquely valuable to assess the assumptions made regarding Re_θ limits. Poll's criteria was experimentally developed on swept cylinders, so the confirmation that these Re_θ limits applied well to a realistic transonic wing in a wind tunnel environment was a significant finding.

However, the frequent occurrence of attachment line bypass transition, especially at the higher Reynolds numbers, made analyzing the crossflow transition characteristics challenging. Maintaining Re_θ values below 100 across the span of the wing could be used to eliminate the large regions of leading-edge transition due to attachment line bypass transition. However, finding a design method that keeps the Re_θ values that low on highly swept wings was previously explored and may not be practical [13]. Additional research should be done to explore new methods of guarding against attachment line bypass transition on wings with high sweep and Reynolds numbers, especially if the chances of incurring surface imperfections in the leading-edge region are higher.

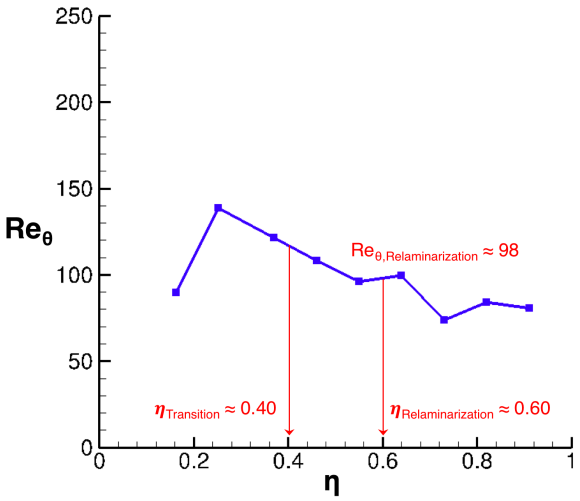

Figure 27. Spanwise distribution of attachment line Re_θ values for the TSP image with leading-edge transition from Figure 26 (M = 0.86, T_T = 40 °F, α = 3.0 deg., and Re_{MAC} = 15.0 million). Markers showing the approximate semispan location of transition and relaminarization are shown. The Re_θ value at relaminarization is approximately 98.

3. Crossflow and Tollmien-Schlichting Transition

To assess the effectiveness of the CATNLF method on delaying transition, a detailed analysis comparing the computational transition characteristics and the experimental transition fronts is required. This subsection will show a sample of the type of analysis that will take place to evaluate crossflow and Tollmien-Schlichting transition on the CRM-NLF wing. A more in-depth analysis will be required to fully assess the method, however, general conclusions can be derived from the results shown here.

The experimental transition front must be determined visually for each data point. The front is generally seen as a straight line of varying x/c locations across the wing. When turbulent wedges are present, it becomes challenging to determine the experimental front. If a front can be seen on both sides of a turbulent wedge, it is assumed that the natural transition would have occurred at that front in the absences of bypass transition. However, if the turbulent wedges become too frequent and coalesce forward of any straight front, the only conclusion that can be made in that region is that natural transition is at least as far aft as the coalescence location. Figure 28 shows an example of an experimental transition front illustrated as a red dashed line overlaid on the TSP image. Once the front is determined, the gridlines are used to estimate the x/c locations of transition at each pressure row. Table 4 lists the approximate transition locations for the example shown in Figure 28. The Reynolds number based on transition location can also be calculated from these transition locations by dimensionalizing the transition x/c locations and multiplying by the experimental unit Reynolds number. An example of these transition Reynolds numbers for each pressure row can also be seen in Table 4.

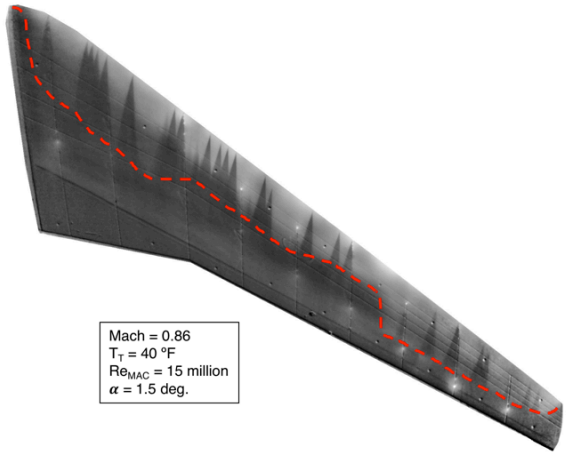

Figure 28. TSP image with the approximated transition front shown (red dashed line) from test condition M = 0.86, T_T = 40 °F, α = 1.5 deg., and Re_{MAC} = 15.0 million.

Table 4. Approximated transition location and transition Reynolds number at each pressure port row based on the transition front from Figure 28 at M = 0.86, T_T = 40 °F, α = 1.5 deg., and Re_{MAC} = 15.0 million.

Row	A	B	C	D	E	F	G	H	I
η	0.163	0.252	0.370	0.460	0.550	0.640	0.730	0.820	0.910
$(x/c)_t$	0.40	0.50	0.40	0.45	0.50	0.35	0.65	0.65	0.60
Re_t (millions)	9.1	10.0	6.2	6.4	6.4	4.0	6.5	5.6	4.3

For the regions of the wing where an experimental transition front can be determined, additional assessment of the crossflow and Tollmien-Schlichting characteristics can be performed. The infilled experimental pressures that correspond to the image are analyzed through the stability analysis and transition prediction software. This software will calculate the N-factor growth of both crossflow and Tollmien-Schlichting, which can then be compared to the approximate experimental transition location at that pressure row. This procedure is performed at each pressure row to gain understanding of the spanwise characteristics of both crossflow and Tollmien-Schlichting transition. One example of N-factor growth is shown in Figure 29 for outboard Row G of the transition front seen in Figure 28. The red marker on the plots represents the approximate experimental transition location at this row. The Tollmien-Schlichting growth remains relatively low across the chord due to a favorable pressure gradient, which was seen consistently on the outboard portion of the wing at the lower angle of attack of 1.5 degrees. The crossflow grows rapidly very near the leading edge, which is typical for wings of high sweep. At the higher angles of attack from the test ($\alpha \geq 2.5$ deg.), the crossflow N-factors reduce rapidly after this initial growth near the leading edge, similar to the design condition shown in Figure 5. However, at the lower angles of attack, such as the 1.5 degrees condition shown here, the crossflow N-factors continue to increase across the chord after the initial growth. The Tollmien-Schlichting growth is lower at the transition location than more forward chord locations, and is also significantly lower than the anticipated critical N-factor. This suggests the dominant mechanism for transition was midchord crossflow growth for the outboard section of the wing at the lower angles of attack from the test ($\alpha \leq 2.0$ deg.). Analyzing the outboard midchord crossflow growth at a variety of Reynolds numbers and angles of attack can help understand the CATNLF method at near-cruise off-design conditions, as well as help characterize the NTF laminar flow testing capabilities, such as determining a crossflow critical N-factor.

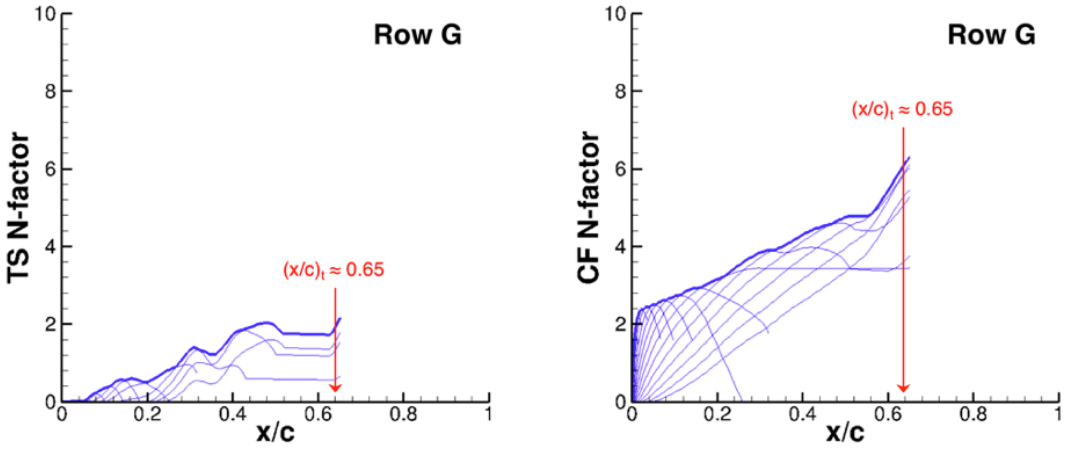

a) TS N-factor growth for outboard Row G. **b) CF N-factor growth for outboard Row G.**

Figure 29. N-factor growth for crossflow (CF) and Tollmien-Schlichting (TS) at outboard Row G. The vertical red marker is the approximated transition location from the corresponding TSP image. The test conditions are M = 0.86, T_T = 40 °F, α = 1.5 deg., and Re_{MAC} = 15.0 million.

Finding test conditions and regions of the wing where different types of transition mechanisms are dominant is advantageous to assessing the CATNLF method. In the previous example, preliminary results suggest midchord crossflow growth is the dominant transition mechanism on the outboard portion of the wing at the lower angles of attack. It is also desirable to identify test conditions where Tollmien-Schlichting growth causes transition. Figure 30 shows a transition front at a higher angle of attack (2.5 deg.) and Reynolds number based on mean aerodynamic chord (17.5 million). At this condition, a significant portion of the wing had leading-edge transition. Additionally, the higher Reynolds number led to additional turbulent wedges. While an image free of bypass transition is preferred, these types

of images can still be used to gain understanding of the CATNLF method. A closer look at Row F shows two turbulent wedges coalescing at approximately x/c = 0.25, which suggests the natural transition location in the absence of bypass transition would be $(x/c)_t > 0.25$. The stability analysis results based on the infilled wind tunnel pressures at Row F corresponding to this image are shown in Figure 31. At this condition, the Tollmien-Schlichting growth increases steadily from the leading edge. The crossflow growth is characteristically similar to the design condition, showing rapid growth near the leading edge that peaks at approximately x/c = 0.05 before decreasing for the remainder of the chord. The transition location for this row was determined to be $(x/c)_t > 0.25$, which is represented by the markers on the N-factor growth plots. The wedges coalescing at this row occurred aft of the crossflow peak, indicating the rapid growth of crossflow at the leading edge did not cause transition. This provides an initial assessment that the CATNLF method is successful in reducing leading-edge crossflow growth using the rapid acceleration. It also implies the leading-edge crossflow critical N-factor is greater than 5 and the Tollmien-Schlichting critical N-factor is greater than 6 for this tunnel condition. These preliminary values are consistent with previously estimated critical N-factors in the NTF [17]. Further analysis at a variety of tunnel conditions is required to provide reasonable estimates to the critical N-factor levels based on the CRM-NLF experiment.

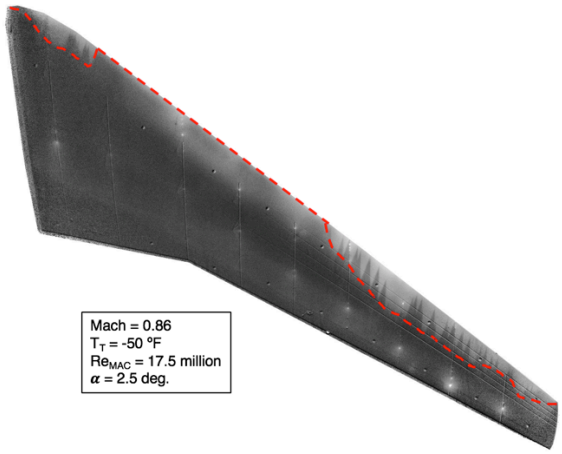

Figure 30. TSP image with the approximated transition front shown (red dashed line) from test condition M = 0.86, T_T = -50 °F, α = 2.5 deg., and Re_{MAC} = 17.5 million.

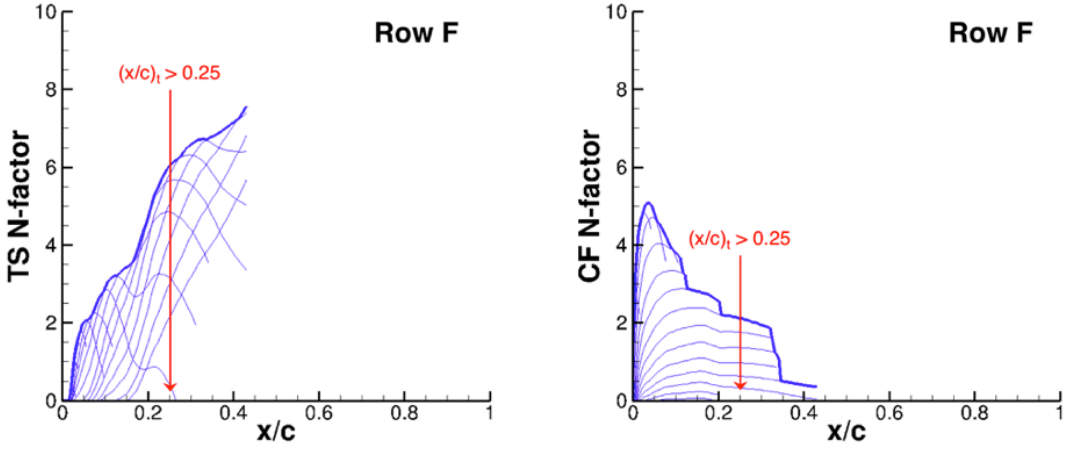

a) TS N-factor growth for Row F. **b) CF N-factor growth for Row F.**

Figure 31. N-factor growth for crossflow (CF) and Tollmien-Schlichting (TS) at outboard Row F. The vertical red marker is the approximated transition location from the corresponding TSP image. The test conditions are M = 0.86, T_T = -50 °F, α = 2.5 deg., and Re_{MAC} = 17.5 million.

4. Preliminary Results in Perspective

Comparing the experimental transition fronts to the pretest CFD transition predictions is of interest to evaluate the computational tools. The pretest CFD fronts are highly dependent on estimated critical N-factors in the wind tunnel and computational pressure distributions. Previous estimates for the Tollmien-Schlichting critical N-factor in the NTF were between 4 and 8, so the design of the model was performed assuming a wind tunnel critical N-factor of 6 for both crossflow and Tollmien-Schlichting. Additional analysis is required to estimate the critical N-factors from the CRM-NLF experiment. However, an initial assessment of the computational tools is performed by comparing the experimental transition front to the computational transition predictions using the previously estimated critical N-factor. The computational pressure distributions analyzed for this comparison are from the pretest CFD condition that most closely matched the experimental pressures. In Figure 32, one of the previous examples of the approximated experimental front (red dashed line) on the TSP image is shown again. Overlaid on this image is the predicted transition front from the pretest CFD (blue solid line). The image shows very close agreement between the wind tunnel front and the pretest CFD predictions. This suggests the computational transition predictions are providing sufficiently accurate transition fronts. It also implies that the previously estimated critical N-factor level of 6 is a reasonable value for this tunnel condition. Additional analysis of the TSP images and pretest CFD results will be needed to fully evaluate the accuracy and consistency of the computational tools used.

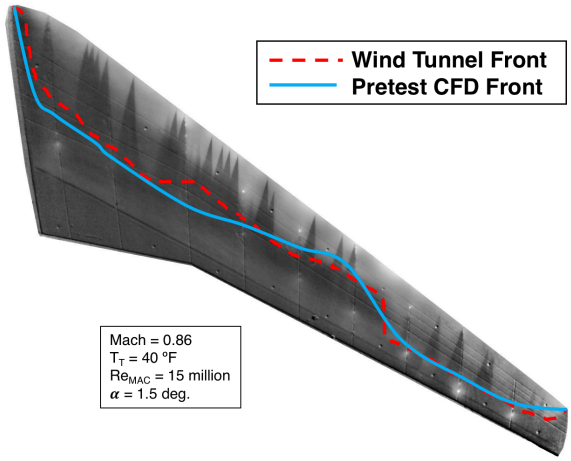

Figure 32. TSP image with the approximated transition front shown (red dashed line) from test condition M = 0.86, T_T = 40 °F, α = 1.5 deg., and Re_{MAC} = 15.0 million. The pre-test CFD transition predictions at corresponding CFD conditions for a critical N-factor of 6 is overlaid on the image.

The CATNLF method was developed to enable NLF on wings with high sweep and Reynolds numbers by attenuating the leading-edge crossflow growth. These wings previously required an LFC system, such as suction, to control the crossflow growth. The historic tradeoff between Reynolds number and leading-edge sweep can be seen in Figure 33. The graph by Malik et al. presents the maximum transition Reynolds number as a function of wing sweep from a variety of NLF experiments dating from 1939 to 2010 [28]. Overlaid on the plot is a symbol corresponding to the maximum transition Reynolds number found thus far in the assessment of the CRM-NLF wind tunnel test. This preliminary maximum of 10 million transition Reynolds number occurred at Mach 0.86, angle of attack of 1.5 degrees, and 15 million chord Reynolds number and was limited by turbulent wedges coalescing. It can be inferred that the CRM-NLF wing would produce higher maximum transition Reynolds numbers in the absence of bypass transition, especially at the higher chord Reynolds numbers. This would require a flight-relevant environment where bypass transition is likely less common and often has a higher critical N-factor. Even so, the initial findings of the CRM-NLF in the NTF nearly doubled the historic maximum transition Reynolds number at comparable sweep angles. While additional analysis is required to fully understand the transition delay technique, these preliminary results suggest the CATNLF method was successful at attenuating crossflow growth that previously led to premature transition.

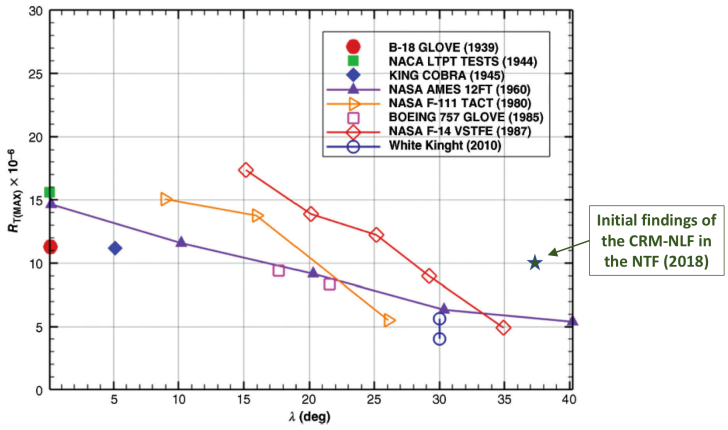

Figure 33. Graph by Malik, et al. showing the maximum transition Reynolds number ($R_{T(max)}$) as a function of wing sweep for a variety of NLF experiments [28]. Overlaid on the plot is the maximum initial findings of the CRM-NLF in the NTF showing the high transition Reynolds numbers achieved during the test relative to historic NLF experiments.

V. Concluding Remarks

An experimental investigation of a new NLF design method took place in the NTF at the NASA Langley Research Center. The new NLF design method, referred to as Crossflow Attenuated NLF (CATNLF), enables significant extents of laminar flow on aircraft components with high sweep and Reynolds numbers, such as the wings of typical commercial transports, that previously required an LFC system. The CATNLF method uses geometry shaping to obtain pressure distributions that control growth of crossflow and Tollmien-Schlichting instabilities. The wind tunnel test aimed to accomplish 3 main goals: validate the CATNLF design method and analysis tools, characterize the NTF laminar flow testing capabilities, and establish best practices for laminar flow wind tunnel testing. In this publication, initial findings are presented relating to the first goal of assessing the CATNLF design method and analysis tools.

The wind tunnel test involved a 5.2% scale semispan model of the new CRM-NLF configuration. The test focused on transonic cruise flight conditions, with the primary data acquired at Mach 0.86, angles of attack from 1.5 to 3 degrees, and chord Reynolds numbers from 10 to 30 million. The semispan model wing was painted with TSP for transition visualization and had a carbon-based heating layer beneath to provide the required temperature gradient for TSP. The data acquired during the test included force and moment measurements, surface static pressure data, transition visualization images, and model deformation information. In this report, a sample of surface static pressure data and transition visualization images are presented and analyzed.

The CATNLF method relies on pressure distributions to delay transition on highly swept wings, so a key requirement for an effective experimental investigation of this method is that the pressure distributions on the model adequately match the desired distributions. A comparison of the experimental and computational pressure distributions is provided in this report. Initial assessment of the data suggests the key features of the CATNLF method were observed in the wind tunnel test. Corrections on Mach and angle of attack were required to provide the best correlation between experimental and computational pressures. The wind tunnel pressure data were infilled with CFD data to enable the use of wind tunnel data in the boundary layer and stability analysis computations.

The strategy to avoid transition due to a turbulent attachment line on the CRM-NLF model is to reduce the attachment line Re_θ values below Poll's criteria of 100 to relaminarize the boundary layer on the inboard section of the wing by locally reducing the leading-edge sweep. Outboard of this reduced sweep region, the only requirement on Re_θ values is to remain below Poll's criteria of 235 for attachment line transition. Transition images showing significant extents of laminar flow verify the use of this strategy for attachment line control. Several images show attachment line bypass transition, which caused full chord loss of laminar flow over a significant spanwise region until the attachment line relaminarized outboard when the Re_θ values fell below 100. Analyzing these images with attachment line bypass transition confirmed the validity of applying Poll's criteria to a transonic wing in a wind tunnel environment, as well as confirmed the computational boundary layer software calculations of Re_θ values.

In this report, transition images acquired during the test are compared to computational transition predictions and stability analysis results to evaluate the CATNLF design method. Transition images are analyzed individually to determine approximate experimental transition fronts for each test condition. The stability analysis results corresponding to infilled wind tunnel pressure data are analyzed and compared to the experimental transition location. Initial results suggest the outboard portion of the CRM-NLF wing is midchord crossflow transition dominant at lower angles of attack, and Tollmien-Schlichting transition dominant at higher angles of attack. Results analyzed thus far show transition Reynolds numbers as high as approximately 10 million on the CRM-NLF wing in the NTF. This preliminary value nearly doubles the published historic values for NLF technologies on components with similar sweep. The initial analysis of the NTF data suggests the CATNLF methodology is a feasible technology to enable NLF on wings with high sweep and Reynolds numbers. The results analyzed thus far support that the NTF is a suitable environment for laminar flow testing in the absence of bypass transition. Future analysis will be completed that continues to assess the effectiveness of the CATNLF method, as well as address the two remaining test goals of characterizing the NTF and establishing best practices for laminar flow wind tunnel testing.

Acknowledgments

This research is funded by the NASA Advanced Air Transport Technology Project within the Advanced Air Vehicles Program. Resources supporting some computational results in this paper were provided by the NASA High-End Computing (HEC) Program through the NASA Advanced Supercomputing (NAS) Division. The authors would like to thank Kyle Goodman and Dr. Sarah Peak, as well as the many instrumentation technicians at the National Transonic Facility, for their invaluable contribution to the acquisition of the experimental data. Additionally, the authors would like to thank Lewis Owens for offering his continued support and expertise in the computational and experimental investigation of boundary layer transition. Finally, the authors thank Donald Saxer, Lonnie Brown, Dr. Richard Wahls, Scott Anders, and Susan Wilz for supporting the planning and execution of the wind tunnel test.

References

[1] Crouch, J., "Boundary-Layer Transition Prediction for Laminar Flow Control (Invited)", 45th AIAA Fluid Dynamics Conference, AIAA AVIATION Forum, AIAA 2015-2472, 2015.

[2] Fujino, M., "Design and Development of the HondaJet", AIAA International Air and Space Symposium and Exposition: The Next 100 Years, AIAA 2003-2530, July 2003.

[3] Anderson, B. T., and Meyer, R. R., "Effects of Wing Sweep on In-Flight Boundary Layer Transition for a Laminar Flow Wing at Mach Numbers from 0.60 to 0.79," NASA TM-101701, 1990.

[4] Joslin, R. D., "Overview of Laminar Flow Control," NASA TP-1998-208705, 1998.

[5] Campbell, R. L., and Lynde, M. N., "Natural Laminar Flow Design for Wings with Moderate Sweep", 34th AIAA Applied Aerodynamic Conference, AIAA AVIATION Forum, AIAA 2016-4326, June 2016.

[6] Lynde, M. N. and Campbell, R. L., "Expanding the Natural Laminar Flow Boundary for Supersonic Transports", 34th AIAA Applied Aerodynamic Conference, AIAA AVIATION Forum, AIAA 2016-4327, June 2016.

[7] Lynde, M. N., and Campbell, R. L., "Computational Design and Analysis of a Transonic Natural Laminar Flow Wing for a Wind Tunnel Model," AIAA-2017-3058, June 2017.

[8] Rivers, M., Lynde, M., Campbell, R., Viken, S., Chan, D., Watkins, A., and Goodliff, S., "Experimental Investigation of the NASA Common Research Model with a Natural Laminar Flow Wing in the NASA Langley National Transonic Facility", 2019 AIAA SciTech Forum, January 2019.

[9] Frink, N.T., Pirzadeh, S.Z., Parikh, P.C., Pandya, M.J., and Bhat, M.K., "The NASA Tetrahedral Unstructured Software System," The Aeronautical Journal, Vol. 104, No. 1040, October 2000, pp.491-499.

[10] Campbell, R. L., "Efficient Viscous Design of Realistic Aircraft Configurations," AIAA-98-2539, June 1998.

[11] Wie, Y.-S., "BLSTA: A Boundary Layer Code for Stability Analysis," NASA CR 4481, 1992.

[12] Chang, C.-L., "The Langley Stability and Transition Analysis Code (LASTRAC): LST, Linear and Nonlinear PSE for 2-D, Axisymmetric, and Infinite Swept Wing Boundary Layers," AIAA 2003-0974, 2003.

[13] Campbell, R. L. and Lynde, M. N., "Building a Practical Natural Laminar Flow Design Capability," AIAA-2017-3059, June 2017.

[14] Poll, D. I. A., "Some Observations of the Transition Process on the Windward Face of a Long Yawed Cylinder," J. Fluid Mech., Vol. 150, 1985, pp. 329-356.

[15] Vassberg, J. C., DeHann, M.A., Rivers, S.M., and Wahls, R.A., "Development of a Common Research Model for Applied CFD Validation", AIAA 2008-6919, August 2008.

[16] Vassberg, J. C., DeHann, M.A., Rivers, S.M., and Wahls, R.A., "Retrospective on the Common Research Model for Computational Fluid Dynamics Validation Studies", Journal of Aircraft, Vol. 55, No. 4, July-August 2018, pp. 1325-1337.

[17] Crouch, J., Sutanto, M., Witkowski, D., Watkins, A., Rivers, M., and Campbell, R., "Assessment of the National Transonic Facility for Natural Laminar Flow Testing", 48th AIAA Aerospace Sciences Meeting Including the New Horizons Forum and Aerospace Exposition, Aerospace Sciences Meetings, AIAA 2010-1302, January 2010.

[18] National Transonic Facility (NTF), "NTF User Guide", NASA Document SP-2011-5-110-LaRC, NASA Langley Research Center, February 2012.

[19] Wahls, R.A., "The National Transonic Facility: A Research Retrospective (Invited)", AIAA 2001-0754, 39th AIAA Aerospace Sciences Meeting and Exhibit, January 2001.

[20] King, R. A., Andino, M. Y., Melton, L., Eppink, J., and Kegerise, M. A., "Flow Disturbance Measurements in the National Transonic Facility", AIAA Journal, Vol. 52, No. 1, January 2014, pp. 116-130.

[21] Goodliff, S.L., Jones, G.S., Balakrishna, S., Chan, D.T., Milholen, W.E., Butler, D., and Cagle, C.M., "Force Measurement Improvements to the National Transonic Facility Sidewall Model Support System", AIAA 2016-0648, January 2016.

[22] Gatlin, G.M., Tomek, W.G., Payne, F.M., and Griffiths, R.C., "Recent Improvements in Semi-Span Testing at the National Transonic Facility (Invited)", AIAA 2006-0508, AIAA, January 2006.

[23] Chan, D., Hooker, J., Wick, A., Plumley, R., Zeune, C., Ol, M., and Demoss, J., "Transonic Semispan Aerodynamic Testing of the Hybrid Wing Body with Over Wing Nacelles in the National Transonic Facility", AIAA 2017-0098, January 2017.

[24] Hammer, M., Popernack, T., Owens, L., and Wahls, R., "Using temperature sensitive paint technology", 40th AIAA Aerospace Sciences Meeting & Exhibit, Aerospace Sciences Meetings, AIAA 2002-0742, 2002.

[25] Klein, C. and Henne, U., "Combination of Temperature Sensitive Paint and Carbon Nanotubes for Transition Detection", 53rd AIAA Aerospace Sciences Meeting, AIAA SciTech, AIAA 2015-1558, January 2015.

[26] Goodman, K.Z., Lipford, W.E., and Watkins, A.N., "Boundary-Layer Detection at Cryogenic Conditions Using Temperature Sensitive Paint Coupled with a Carbon Nanotube Heating Layer", *Sensors* 2016, 16, 2062.

[27] Watkins, A.N., Goodman, K.Z., and Peak, S.M., "Transition Detection at Cryogenic Temperatures Using a Carbon-Based Resistive Heating Layer Coupled with Temperature Sensitive Paint", 2019 AIAA SciTech Forum, January 2019.

[28] Malik, M.R., Crouch, J.D., Saric, W.S., Lin, J.C., and Whalen, E.A., "Application of Drag Reduction Techniques to Transport Aircraft", Encyclopedia of Aerospace Engineering, 2015.